 doi:10.20944/preprints202005.0250.v10

Article

Early Universe Plasma Separation and the Creation of a Dual Universe ‡

Mohammed B. Al-Fadhli [1,*]

[1] College of Science, University of Lincoln, Lincoln, LN6 7TS, UK.
* Correspondence: malfadhli@lincoln.ac.uk; mo.fadhli7@gmail.com.
‡ This paper is an extended version from the proceeding paper: Al-Fadhli, M. B. On Spacetime Duality and Bounce Cosmology of a Dual Universe. In Proceedings of the 1st Electronic Conference on Universe, 22–28, Feb 2021.

Abstract: The recent Planck Legacy release confirmed the presence of an enhanced lensing amplitude in the cosmic microwave background (CMB) power spectra, which prefers a positively curved early Universe with a confidence level exceeding 99%. In this study, the pre-existing curvature is incorporated to extend the field equations where the derived wavefunction of the Universe is utilised to model Universe evolution with reference to the scale factor of the early Universe and its radius of curvature upon the emission of the CMB. The wavefunction reveals both positive and negative solutions, implying that matter and antimatter of early Universe plasma evolved in opposite directions as distinct Universe sides, corroborating the axis of CMB. The wavefunction indicates that a nascent hyperbolic expansion away from early plasma is followed by a first phase of decelerating expansion during the first ~10 Gyr, and then, a second phase of accelerating expansion in reverse directions, whereby both sides free-fall towards each other under gravitational acceleration. The predicted conformal curvature evolution demonstrates the fast orbital speed of outer stars owing to external fields exerted on galaxies as they travel through conformally curved space-time. Finally, the wavefunction predicts an eventual time-reversal phase comprising rapid spatial contraction that culminates in a Big Crunch, signalling a cyclic Universe. These findings show that early plasma could be separated and evolved into distinct sides of the Universe that collectively inducing its evolution, physically explaining the effects attributed to dark energy and dark matter.

Keywords: Duality; Antimatter; Extended General Relativity; String Theory Branes.

Local knowledge lies in the duality of apprehender and apprehended (Relativism).

Global/absolute knowledge might be out of the apprehender's reach except its local influence.

1. Introduction

The Planck Collaboration released in 2018 the final and most thorough spectrum of the cosmic microwave background (CMB), the first light in the Universe [1]. Astrophysical observations and theoretical frameworks have established that the early Universe was composed of hot and very dense plasma comprising equal quantities of matter and antimatter [2]. Antimatter is presumed to have been eliminated through early annihilation processes within the assumption of matter-antimatter asymmetry, which motivated by the apparent missing of antimatter in the observable Universe and experimental findings of violations in the parity conservation [3,4]. However, recent advanced measurements of the fine structure of hydrogen and antihydrogen atoms were found to be consistent with the Quantum Electrodynamics theory predictions, including the Lamb-shift feature [5,6]. This can endorse the concept of identical matter and antimatter apart of their opposite charge and spin, which undermines the elimination assumption. In addition, the recent observations of parity violations from the CMB [7] could indicate a sided Universe; thus, the experimentally measured parity violations can be an implication of a sided Universe, not an intrinsic asymmetry between matter and antimatter.

 doi:10.20944/preprints202005.0250.v10

Alternatively, matter and antimatter of early Universe plasma could be separated in the presence of primordial electromagnetic fields due to the phenomenon of plasma drift; thereby evolving in opposite directions owing to their opposite spin and charge, where the magnetic fields that presently pervade the Universe at all probed scales favour a primordial origin of such kind [8–10]. The separation under and until the right conditions would allow the closed early plasma, as revealed by Planck release [11], to achieve thermal equilibrium in accordance with the CMB observations [4]. In this sense, the generated electromagnetic forces on matter and antimatter can induce a nascent expansion in opposite directions countering strong gravitational forces of early Universe very dense plasma while the residual annihilation processes could augment the expansion rate [12,13].

In addition, the necessity of the dark energy and dark matter in the present Universe could be a consequence of the antimatter elimination assumption in the early Universe. Currently, the presumed concepts of dark energy and dark matter, as well as the isotropy, homogeneity, and the spatial flatness of the Universe, are being challenged by new observations and precise measurements. In 2020, Riess found the expansion of the Universe is faster than that estimated by the standard lambda cold dark matter model (ΛCDM), with the disagreement between several independent measurements obtained from the early Universe using ΛCDM based on CMB data and from the present Universe using the type Ia supernovae (SNe Ia) distance redshift direct method is being four to six standard deviations [14–19]. This adds up to the well-known vacuum catastrophe that the predicted value of the cosmological constant in the ΛCDM contradicts the predictions of the Quantum Field theory (QFT) where the discrepancy is about 120 orders of magnitude [20–23]. Ryskin in 2020 disproved vacuum energy as the cause of the accelerated expansion of the Universe [24]. Regarding dark matter, in addition to the observed baryonic Tully-Fisher relation [25,26], external fields that influence galactic rotation curves were detected with a confidence level up to eleven-sigma [27]. Further, the cosmic shear observed by the Kilo Degree Survey 450 is conflicting with the Planck datasets at about two standard deviations [28] with the amplitude of matter power spectrum is statistically in conflict [29–31]. These observations naturally preferring modified gravity theories [32–37] of modified background or an effective Newtonian 'constant' G_{eff} [29,30]. However, the observed gravitational lensing in the collusion of the Bullet Cluster [38–40] indicates the incompleteness of current modified gravity theories. Further, the observed super-voids, walls and galaxy filaments show an inhomogeneous Universe [41] while the fine structure 'constant' evolution in both time and across a specific axis [42], the observed preferred direction in the Universe by several independent surveys using different instruments and techniques [43], and the variation of the expansion rate of the Universe depending on the direction [44] indicate a strong anisotropy at a five-sigma confidence level [41,44,45]. Moreover, the CMB anomalies [46], curiosities of baryon acoustic oscillations (BAO) [47,48] and the high cluster collision velocities contradict the ΛCDM concordance cosmology [49]. [1]

Furthermore, the Planck Legacy 2018 (PL18) release has confirmed the existence of an enhanced lensing amplitude in the power spectra of the CMB that is more than that estimated by the ΛCDM, which favours a positive curvature of the early Universe with a confidence level more than 99% [11,50,51]. Although the flat Universe could be recovered by combining the PL18 release with CMB lensing and BAO data, the curvature parameter tension is calculated to be 2.5 to 3-sigma using a possibly unreliable statistic [50]. Whereas the early positive curvature is preferred by PL18 and can naturally elucidate the anomalous lensing amplitude [11], its confirmation remains arguably under further studies and investigations. In addition, the observed gravitational lensing by substructures of several galaxy clusters at an order of magnitude higher than that estimated by the ΛCDM [52,53] can provide another indication of the curvature from the modern Universe. Thus, these findings favour a closed Universe despite the present/local space-time flatness.

[1] Emerging evidence and new challenges highlight the growing need for a profound adjustment to ΛCDM and its framework or new physics for the current precise cosmology era [54].

 doi:10.20944/preprints202005.0250.v10

In contrast with the PL18 and gravitational lensing signs of a closed Universe, the flat Universe assumption seems to be originated from General Relativity (GR) postulation that spacetime is basically flat while the presence of energy density is the main source of its curvature. Although GR has passed numerous tests, its predictions are still questionable at high curvature regimes while its lost boundary term, incompatibility with Quantum Mechanics and the necessity of dark matter/energy can indicate its incompleteness [55–57].

Accordingly, in this study, a closed early Universe model is considered where the pre-existing curvature is incorporated to extend GR's field equations and to approach the problems of accelerated expansion and fast orbital speed of outer stars from a new perspective. The closed finite Universe could aid a large-scale cut-off in primaeval density fluctuations, provide an agreement with low CMB anisotropy observations [46,58] and explain the quantum entanglement, where the total Universe energy is finite; thus, cosmic conservation preserves the total spin of a pair of particles regardless of their locations; otherwise, unconserved total spin of the pair would violate the finite Universe energy [59]. This paper is organised as follows. Section 2 presents the extended field equations, and sections 3 and 4 discuss the Universe model and its evolution. Section 5 presents spiral galaxy formation and rotation. Sections 6 discusses the Universe minimal radius. Finally, Section 7 concludes this work and suggests future works.

2. Extended Field Equations for a Curved Universe: Extended General Relativity

The recent PL18 release has preferred the positively curved early Universe, that is, is a sign of a pre-existing/background curvature. To consider this pre-existing curvature and its evolution over cosmic time, a modulus of space-time deformation/curvature, E_D, is introduced based on the Elasticity theory [60]. By utilising the trace-reversed Einstein field equations, the modulus $E_D =$ (stress/strain) can be expressed as

$$E_D = \frac{T_{\mu\nu} - T g_{\mu\nu}/2}{R_{\mu\nu}/\mathcal{R}} = \frac{\mathrm{c}^4}{8\pi G_t {r_t}^2} \tag{1}$$

where the stress is signified by the stress-energy momentum tensor $T_{\mu\nu}$ of trace T while the strain is signified by the Ricci curvature tensor $R_{\mu\nu}$ as the change in the curvature divided by the scalar of the pre-existing curvature $\mathcal{R} = 1/{r_t}^2$; r_t is the Universe's radius of curvature as a function of cosmic time, t, and $g_{\mu\nu}$ is the metric tensor. According to the Elasticity theory, E_D is a constant [60]; thus, Eq. (1) shows an inverse proportionality between the gravitational 'constant' G_t and r_t, where G_t follows the inverse square law with respect to the Universe radius. This relationship is consistent with Mach's principle, the reliance of the small structure on the larger structure. Schrödinger in 1925 pointed to the reliance of G_t on the distribution of the Universe's masses and its radius while Dirac in 1938 proposed its correlation to the Universe age [61]. The evolution in G_t is preferred to reduce the conflict of matter power spectrum amplitude with Planck datasets [27,29,30] while the decrease in star formation rate over the Universe age [62] can be due to the decrease in G_t over cosmic time. Experimental measurements of G_t suggested its change over time [63] while the gradual evolution in the fine-structure 'constant' [42,64,65] can reveal that the presumed fundamental constants rely on other Universe properties.

In contrast, E_D is in terms of energy density and represents the resistance of the continuum (space-time continuum [2]) to deformation, where the law of energy conservation is a firm fundamental law [60]. Eq. (1) shows E_D is proportional to the fourth-power of the speed of light, which in turn is directly proportional to the frequency; in accordance with the frequency cut-off predictions of the vacuum energy density in QFT [23,66]; thus, E_D characterizes spacetime resistance to curvature and can represent vacuum energy density.

[2] Space-time can be regarded as a continuum with a dual quantum nature, that it curves as waves according to the GR while fluxing as quantum energy particles; the latter is justified because the energy flux from early Universe plasma into space at the speed of light creating a 'space-time continuum' or 'vacuum energy'. This could be corroborated by light polarisation from CMB [7].

Preprints (www.preprints.org) | NOT PEER-REVIEWED | Posted: 21 June 2021 doi:10.20944/preprints202005.0250.v10

By incorporating the pre-existing/background curvature and complying with the energy conservation law, the Einstein–Hilbert action is extended to

$$S = \int \left[\frac{E_D}{2}\frac{R}{\mathcal{R}} + \mathcal{L}_M\right]\sqrt{-g}\, d^4x \tag{2}$$

where R and $\mathcal{R}$ are the Ricci/induced and the pre-existing scalar curvatures respectively, $\mathcal{L}_M$ is the Lagrangian density and g is the determinant of the metric tensor g_{uv}. The indistinctive variation in the action yields

$$\delta S = \int \left[\frac{E_D}{2}\left(\frac{\delta R\sqrt{-g}}{\mathcal{R}} - \frac{\delta\mathcal{R}\sqrt{-g}}{\mathcal{R}^2}R + \frac{\delta\sqrt{-g}}{\mathcal{R}}R\right) + \left(\delta\mathcal{L}_M\sqrt{-g} + \delta\sqrt{-g}\mathcal{L}_M\right)\right] d^4x \tag{3}$$

The variation in the scalar curvature, $R = R_{\mu\nu}g^{\mu\nu}$, is $\delta R = R_{\mu\nu}\delta g^{\mu\nu} + g^{uv}\delta R_{\mu\nu}$ while by utilising Jacobi's formula for the differentiation of the determinant; accordingly, $\delta\sqrt{-g} = -\sqrt{-g}\, g_{\mu\nu}\delta g^{\mu\nu}/2$ where the variation in $g_{\mu\nu}g^{\mu\nu} = \delta^{\mu}_{\nu}$ is $g_{\mu\nu}\delta g^{\mu\nu} = -g^{\mu\nu}\delta g_{\mu\nu}$ [67]. Hence, the variation in the action is expanded to

$$\delta S = \int \left[\begin{array}{l} \frac{E_D}{2}\left(\frac{R_{\mu\nu}\delta g^{\mu\nu} + g^{\mu\nu}\delta R_{\mu\nu}}{\mathcal{R}} - \frac{\mathcal{R}_{\mu\nu}\delta g^{\mu\nu} + g^{\mu\nu}\delta\mathcal{R}_{\mu\nu}}{\mathcal{R}^2}R - \frac{g_{\mu\nu}\delta g^{\mu\nu}}{2\mathcal{R}}R\right) \\ + \left(\delta\mathcal{L}_M - \frac{g_{\mu\nu}\delta g^{\mu\nu}}{2}\mathcal{L}_M\right) \end{array}\right]\sqrt{-g}\, d^4x \tag{4}$$

By considering the first boundary term, $\int (E_D/2\mathcal{R})g^{\mu\nu}\delta R_{\mu\nu}\sqrt{-g}\, d^4x$. The variation in the Ricci curvature tensor δR_{uv} can be expressed in terms of the covariant derivative of the difference between two Levi-Civita connections, the Palatini identity: $\delta R_{\mu\nu} = \nabla_\rho\left(\delta\Gamma^{\rho}_{\nu\mu}\right) - \nabla_v\left(\delta\Gamma^{\rho}_{\rho\mu}\right)$, where this variation with respect to the inverse metric $g^{\mu\nu}$ can be obtained by using the metric compatibility of the covariant derivative, $\nabla_\rho g^{\mu\nu} = 0$ [67], as $g^{\mu\nu}\delta R_{\mu\nu} = \nabla_\rho\left(g^{\mu\nu}\delta\Gamma^{\rho}_{\nu\mu} - g^{\mu\rho}\delta\Gamma^{\sigma}_{\sigma\mu}\right)$. Thus, the first boundary term as a total derivative for any tensor density is transformed based on Stokes' theorem with renaming the dummy indices as

$$\begin{aligned} &\frac{E_D}{2\mathcal{R}}\int g^{\mu\nu}\delta R_{\mu\nu}\sqrt{-g}\, d^4x = \frac{E_D}{2\mathcal{R}}\int \nabla_\rho\left(g^{\mu\nu}\delta\Gamma^{\rho}_{\nu\mu} - g^{\mu\rho}\delta\Gamma^{\sigma}_{\sigma\mu}\right)\sqrt{-g}\, d^4x \\ &\equiv \frac{E_D}{2\mathcal{R}}\iiint_{\mathcal{M}} \nabla_\mu A^\mu\sqrt{-g}\, d^4x = \frac{E_D}{2\mathcal{R}}\oiint_S A^\mu.\hat{n}_u\sqrt{|q|}\, dS = \frac{E_D}{2\mathcal{R}}\oint_{\partial\mathcal{M}} K\epsilon\sqrt{|q|}\, d^3x \end{aligned} \tag{5}$$

The non-boundary term $E_D/2\mathcal{R}$ is left outside the integral transformation as it only acts as a scalar to the integral called S_{GHY} [68,69]. The same is applied to the second boundary term in Eq. (4). Accordingly, the variation in the action is expressed as

$$\delta S = \int \left[\begin{array}{l} \frac{E_D}{2}\left(\frac{R_{\mu\nu}\delta g^{\mu\nu}}{\mathcal{R}} - \frac{\mathcal{R}_{\mu\nu}\delta g^{\mu\nu}}{\mathcal{R}^2}R - \frac{g_{\mu\nu}\delta g^{\mu\nu}}{2\mathcal{R}}R\right) \\ + \left(\frac{2\delta\mathcal{L}_M/\delta g^{\mu\nu} - g_{\mu\nu}\mathcal{L}_M}{2}\delta g^{\mu\nu}\right) \end{array}\right]\sqrt{-g}\, d^4x + \int\left[\frac{E_D\epsilon}{2}\left(\frac{K\sqrt{|q|}}{\mathcal{R}} - \frac{\mathcal{K}\sqrt{|p|}}{\mathcal{R}^2}R\right)\right] d^3x \tag{6}$$

where K and $\mathcal{K}$ are the traces of the induced and the pre-existing/conformal extrinsic curvatures respectively, q and p are the determinants of their induced metric tensors respectively and ϵ equals 1 when the normal $\hat{n}_u$ is a spacelike entity and equals -1 when it is a timelike entity. It is worth noting that after applying the integral transformation, the matter and curvature actions are satisfying the criteria that the variation in the action δS is with respect to the variation in the inverse metric $\delta g^{\mu\nu}$ excluding the boundary action that still lacks this feature. Thus, to achieve the consistency of the action, the variation in

Preprints (www.preprints.org) | NOT PEER-REVIEWED | Posted: 21 June 2021 doi:10.20944/preprints202005.0250.v10

the boundary action has to be determined. The indistinctive variation is the first term is

$$\frac{E_D\epsilon}{2\mathcal{R}}\int\left(K_{\mu\nu}\delta q^{\mu\nu}+q^{\mu\nu}\delta K_{\mu\nu}+K\frac{\delta\sqrt{|q|}}{\sqrt{|q|}}\right)\sqrt{|q|}\,d^3x \tag{7}$$

where $K=K_{\mu\nu}q^{\mu\nu}$. The non-boundary term $E_D\epsilon/2\mathcal{R}$ is left outside, where it can be considered as a scalar. Otherwise, its high-order variational terms can be incorporated into the conformal transformation function Ω^2 as follows. By utilising Jacobi's formula for the determinant differentiation; thus, $\delta\sqrt{|q|}=-\sqrt{|q|}\,q_{\mu\nu}\delta q^{\mu\nu}/2$ while the variation in the $q^{\mu\nu}q_{\mu\nu}=\delta^{\mu}_{\nu}$ can be expressed as $q^{\mu\nu}=-q_{\mu\nu}\delta q^{\mu\nu}/\delta q_{\mu\nu}$; thus, the boundary term is

$$\frac{E_D\epsilon}{2\mathcal{R}}\int\left(K_{\mu\nu}\delta q^{\mu\nu}-\frac{1}{2}K\left(q_{\mu\nu}\delta q^{\mu\nu}+2q_{\mu\nu}\frac{\delta K_{\mu\nu}}{\delta q_{\mu\nu}K}\delta q^{\mu\nu}\right)\right)\sqrt{|q|}\,d^3x \tag{8}$$

here $\delta K_{\mu\nu}/\delta q_{\mu\nu}K=(\delta K_{\mu\nu}/K_{\mu\nu})(q_{\mu\nu}/\delta q_{\mu\nu})=\delta\ln K_{\mu\nu}/\delta\ln q_{\mu\nu}$ resembles the Ricci flow in a normalised form reflecting the conformal distortion in the boundary, which can be expressed as a positive function Ω^2 based on Weyl's conformal transformation [70] as $\tilde{q}_{\mu\nu}=q_{\mu\nu}\Omega^2$. Therefore, Eq. (8) can be expressed as

$$\frac{E_D\epsilon}{2\mathcal{R}}\int\left(K_{\mu\nu}\delta q^{\mu\nu}-\frac{1}{2}K\hat{q}_{\mu\nu}\delta q^{\mu\nu}\right)\sqrt{|q|}\,d^3x \tag{9}$$

where $\hat{q}_{\mu\nu}=q_{\mu\nu}+2\tilde{q}_{\mu\nu}$ is the conformal transformation of the induced metric tensor where Einstein spaces are a subclass of the conformal space [71]. The same is applied for the second boundary term, thus, the variation in the full action is

$$\delta S=\int\begin{matrix}\left[\frac{E_D}{2}\left(\frac{R_{\mu\nu}}{\mathcal{R}}-\frac{\mathcal{R}_{\mu\nu}}{\mathcal{R}^2}R-\frac{g_{\mu\nu}}{2\mathcal{R}}R\right)+\frac{2\delta\mathcal{L}_M/\delta g^{\mu\nu}-g_{\mu\nu}\mathcal{L}_M}{2}\right]\delta g^{\mu\nu}\sqrt{-g}\,d^4x+\\ \left[\frac{E_D\epsilon}{2}\frac{K_{\mu\nu}-\frac{1}{2}K\hat{q}_{\mu\nu}}{\mathcal{R}}\right]\delta q^{\mu\nu}\sqrt{|q|}\,d^3x-\left[\frac{E_D\epsilon}{2}\frac{\mathcal{K}_{\mu\nu}-\frac{1}{2}\mathcal{K}\hat{p}_{\mu\nu}}{\mathcal{R}^2}R\right]\delta p^{\mu\nu}\sqrt{|p|}\,d^3x\end{matrix} \tag{10}$$

The stress-energy momentum tensor, $T_{\mu\nu}$, is proportional to the Lagrangian term by definition as $T_{\mu\nu}:=\mathcal{L}_M g_{\mu\nu}-2\delta\mathcal{L}_M/\delta g^{\mu\nu}$ [67,72]; thus, by implementing ϵ as a timelike entity and applying the principle of stationary action, the extended field equations are

$$\frac{R_{\mu\nu}}{\mathcal{R}}-\frac{1}{2}\frac{R}{\mathcal{R}}g_{\mu\nu}-\frac{R}{\mathcal{R}^2}\mathcal{R}_{\mu\nu}+\frac{R\left(\mathcal{K}_{\mu\nu}-\frac{1}{2}\mathcal{K}\hat{p}_{\mu\nu}\right)-\mathcal{R}\left(K_{\mu\nu}-\frac{1}{2}K\hat{q}_{\mu\nu}\right)}{\mathcal{R}^2}=\frac{T_{\mu\nu}}{E_D} \tag{11}$$

The conformal curvature term comprising $\mathcal{R}_{\mu\nu}$ accounts for the pre-existing/conformal curvature evolution over cosmic time, where $\mathcal{R}_{\mu\nu}/\mathcal{R}=\mathcal{R}_{\mu\nu}/\mathcal{R}_{\mu\nu}\tilde{g}^{\mu\nu}=\tilde{g}_{\mu\nu}$ is in correspondence with Weyl's conformal transformation of the metric [70,71], where the conformal transformation can describe the tidal distortion and the gravitational waves in the absence of matter [73]. On the other hand, the boundary term comprising $\mathcal{K}_{\mu\nu}$ accounts for the conformal evolution of the extrinsic curvature of the background/global boundary over cosmic time while term comprising $K_{\mu\nu}$ accounts for the induced evolution of the extrinsic curvature of local relativistic boundary of celestial objects. [3]

[3] The Brane notion to higher dimensions in the String Theory can be reconstructed in form of a local relativistic 4D space-time represented by the relativistic term comprising $R_{\mu\nu}$ of extrinsic local boundary $K_{\mu\nu}$ that is embedded and travelling through an absolute global 4D space-time background represented by the conformal term comprising $\mathcal{R}_{\mu\nu}$ of extrinsic global $\mathcal{K}_{\mu\nu}$ boundary. This can be interrupted as a local relativistic gas cloud of local boundary travelling and spinning through the global absolute background. See Figure 6 for more details.

Preprints (www.preprints.org) | NOT PEER-REVIEWED | Posted: 21 June 2021 doi:10.20944/preprints202005.0250.v10

The extended field equations in Eqs. (11) can be interpreted as indicating that the induced curvature over the pre-existing curvature equals the ratio of the imposed energy density and its flux to the vacuum energy density and its flux through an expanding/contracting Universe. By substituting Eq. (1) to Eqs. (11), the field equations can be simplified to

$$R_{\mu\nu} - \frac{1}{2}R\hat{g}_{\mu\nu} + \frac{R\left(\mathcal{K}_{\mu\nu} - \frac{1}{2}\mathcal{K}\hat{p}_{\mu\nu}\right) - \mathcal{R}\left(K_{\mu\nu} - \frac{1}{2}K\hat{q}_{\mu\nu}\right)}{\mathcal{R}} = \frac{8\pi G_t}{c^4}T_{\mu\nu} \tag{12}$$

where $\hat{g}_{\mu\nu} = g_{\mu\nu} + 2\tilde{q}_{\mu\nu}$. The boundary term is only significant at high-energy limits such as within black holes [68]. The evolution in G_t can accommodate the pre-existing curvature evolution over cosmic time against constant G for a special flat space-time case. The extended equations can remove singularities and satisfy a conformal invariance theory. [4]

3. Closed Early Universe Model

The Friedmann–Lemaître metric is the standard cosmological metric model, which assumes an isotropic and homogenous Universe [74,75], where the isotropy and homogeneity of early Universe plasma based on the CMB are consistent with this metric. The PL18 indicated a closed early Universe; thus, the plasma reference radius of curvature r_P upon the emission of the CMB and the corresponding early Universe scale factor a_P at the reference cosmic time t_p are incorporated to reference this metric shown in Figure 1.

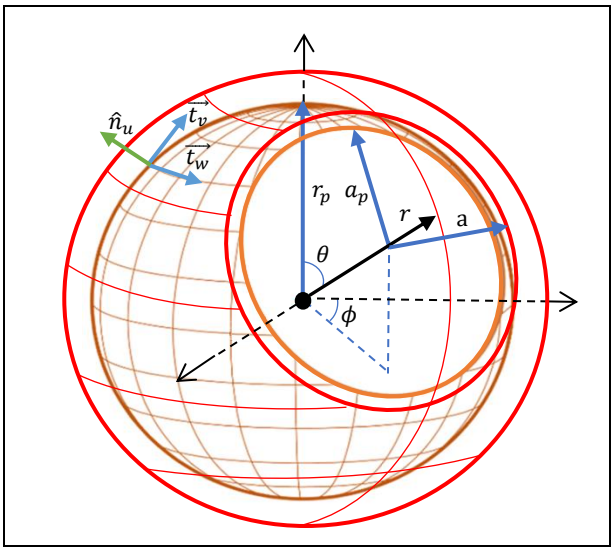

Figure 1. The hypersphere of a positively curved early Universe plasma expansion upon the CMB emissions. r_p is the reference radius of the intrinsic curvature and a_p is the reference scale factor of the early Universe. $\hat{n}_u$ and $\vec{t}_v$ are the normal and tangential vectors on the manifold boundary respectively regarding the extrinsic curvature.

Hence, the four-dimension spacetime interval of the referenced metric tensor $g_{\mu\nu}$ is

$$ds^2 = c^2\,dt^2 - \frac{a^2}{{a_p}^2}\left(\frac{dr^2}{1 - \frac{r^2}{{r_p}^2}} + r^2\,d\theta^2 + r^2 sin^2\theta\,d\phi^2\right) \tag{13}$$

where a/a_p is a new dimensionless scale factor.

[4] As the Universe expands over the cosmic time (over its age), i.e., its radius of curvature r_t increases and thus the pre-existing/background curvature, $\mathcal{R} = 1/{r_t}^2$, decreases. Thus, the curvature of the background is independent from the local relativistic curvature, R, induced by the presence of energy density. The absolute global time could bring compatibility with the Quantum Mechanics and facilitate the quantization of the local relativistic gravitational fields.

Preprints (www.preprints.org) | NOT PEER-REVIEWED | Posted: 21 June 2021 doi:10.20944/preprints202005.0250.v10

The Ricci curvature tensor and Ricci scalar curvature are solved using Christoffel symbolls of the second kind for g_{uv} in Eq. (13) (derivations in Appendix A; no conformal transformation is included, therefore, its outcomes are comparable with the literature while well-defined Christoffel symbols for the conformally transformed metric are in Appendix B):

$$R_{tt} = -3\frac{\ddot{a}}{a}, \qquad R_{rr} = \frac{1}{c^2}\left(\frac{a\ddot{a}}{{a_p}^2} + \frac{2\dot{a}^2}{{a_p}^2} + \frac{2c^2}{{r_p}^2}\right)/\left(1 - \frac{r^2}{{r_p}^2}\right),$$
$$R_{\theta\theta} = \frac{r^2}{c^2}\left(\frac{a\ddot{a}}{{a_p}^2} + \frac{2\dot{a}^2}{{a_p}^2} + \frac{2c^2}{{r_p}^2}\right), \qquad R_{\phi\phi} = \frac{r^2 sin^2\theta}{c^2}\left(\frac{a\ddot{a}}{{a_p}^2} + \frac{2\dot{a}^2}{{a_p}^2} + \frac{2c^2}{{r_p}^2}\right), \tag{14}$$

The Ricci scalar curvature is

$$R = R_{\mu\nu}\, g^{\mu\nu} = -\frac{6}{c^2}\left(\frac{\ddot{a}}{a} + \frac{\dot{a}^2}{a^2} + \frac{c^2\, {a_p}^2}{a^2\, {r_p}^2}\right). \tag{15}$$

where the dotes are cosmic time derivatives. By solving the field equations for a perfect fluid given by $T_{\mu\nu} = (\rho + P/c^2)\, u_\mu u_\nu + P g_{\mu\nu}$ [67,72,76] and substituting Eqs. (13-15), the Friedmann equations that count for the plasma reference radius and reference scale factor:

$$H^2 \equiv \frac{\dot{a}^2}{a^2} = \frac{8\pi G_t\, \rho}{3} - \frac{c^2\, {a_p}^2}{a^2\, {r_p}^2}, \tag{16}$$

$$\dot{H} \equiv \frac{\ddot{a}}{a} = -\frac{4\pi G_t}{3}\left(\rho + 3\frac{P}{c^2}\right). \tag{17}$$

where H, P, and ρ are Hubble parameter, pressure, and density respectively. By utilising the imaginary cosmic time, $\tau = it$, the referenced Friedman equations can be solved at the reference time τ_p by rewriting Eq. (16) in terms of the conformal time in its parametric form, $d\eta = -i\frac{a_p}{a}d\tau$ (where $\dot{a} = i\frac{da}{d\tau}$); thus, $d\eta = \frac{a_p}{a\dot{a}}da$:

$$\int_0^\eta d\eta = \int_0^{2\pi} a_p \left(\frac{8\pi G_p \rho_p {a_p}^3}{3} a - \frac{c^2 {a_p}^2}{{r_p}^2} a^2\right)^{-1/2} da \tag{18}$$

where $\rho = \frac{\rho_p {a_p}^3}{a^3}$ [77] and $G_t = G_p$, the gravitational parameter at τ_p. By integrating, the scale factor evolution is

$$a(\eta)/a_p = \frac{M_p G_p}{c^2 r_p}\left(1 - cos\frac{c}{r_p}\eta\right) \tag{19}$$

where $M_p = \frac{4}{3}\pi\rho_p {r_p}^3$ is the early plasma mass. In addition, the evolution of the imaginary time $\tau(\eta)$ can be obtained by integrating the length of the spatial scale factor contour over the expansion speed H_η while initiating at the reference imaginary time τ_p with the corresponding scale factor a_p. Thus, by rewriting Eq. (19) in terms of the Hubble parameter by its definition and initiating at τ_p as $d\tau = i\frac{da(\eta)}{H_\eta a_p}$:

$$\int_{\tau_P}^{\tau} d\tau = i\int_0^\eta \frac{M_p G_p}{c^2 r_p}\left(1 - cos\frac{c}{r_p}\eta\right)d\eta \tag{20}$$

By integration, the evolution of the imaginary time is

$$\tau(\eta) = i\frac{E}{6H_\eta E_D}\left(\eta - sin\frac{c}{r_p}\eta\right) + \tau_p \tag{21}$$

where the constant in Eqs. (23) has been rewritten in terms of the modulus E_D representing the vacuum energy density and the Universe energy density E by using Eq. (1).

Preprints (www.preprints.org) | NOT PEER-REVIEWED | Posted: 21 June 2021 doi:10.20944/preprints202005.0250.v10

According to the law of energy conservation, the covariance divergence of the stress-energy tensor vanishes, $\Delta_v T^{uv}$, thus, $\frac{\dot{a}}{a} T_u^u + 3\frac{\dot{a}}{a}\rho - i\frac{\partial\rho}{\partial\tau} = 0$, $3\left(\rho + \frac{P}{c^2}\right)\frac{\dot{a}}{a} - i\frac{\partial\rho}{\partial\tau} = 0$. By combining these outcomes, integrating, and substituting the spatial scale factor rate in Eq. (19) to their outcome, the matter density evolution is

$$\rho_m(\eta) = D_p\left(1 - cos\frac{c}{r_p}\eta\right)^{-3} \tag{22}$$

where D_p is constant. According to Eq. (17), the acceleration/deceleration of the Universe expansion, $\ddot{a}$, relies on the evolution in both Universe's density and its scale factor. Thus, by substituting Eqs. (22, 19) to Eq. (17), $\ddot{a}$ is

$$\ddot{a}(\eta) = -\frac{4\pi G_t}{3} D_p\left(1 - cos\frac{c}{r_p}\eta\right)^{-3}\frac{E}{6E_D}a_p\left(1 - cos\frac{c}{r_p}\eta\right) \tag{23}$$

The Hubble parameter, H, can be obtained by integrating the acceleration, $\ddot{a}$, over the conformal time while initiating at τ_p with the corresponding scale factor a_p. Therefore, by rewriting Eq. (23) in terms of the Hubble parameter rate, $\dot{H}$, by its definition at τ_p as follows

$$\int_{H_P}^{H}\dot{H} = \int_0^{\eta} -\frac{2\pi G_p E D_p}{9E_D}\left(1 - cos\frac{c}{r_p}\eta\right)^{-2} d\eta \tag{24}$$

By integrating using the Weierstrass substitution (the tangent half-angle substitution), the Hubble parameter is

$$H_{\eta,m} = H_m\left(\frac{1}{3}cot^3\frac{c}{2r_p}\eta + cot\frac{c}{2r_p}\eta\right) + H_p \tag{25}$$

where H_m and H_p are the integration constants. Since radiation propagates faster than matter. The Hubble parameter evolution for radiation-only can be obtained by using the same procedure in Eqs (22-25) as

$$H_{\eta,r} = H_r\left(\frac{1}{5}cot^5\frac{c}{2r_p}\eta + \frac{2}{3}cot^3\frac{c}{2r_p}\eta + cot\frac{c}{2r_p}\eta\right) + H_p \tag{26}$$

where H_r is the integration constant.

The quantized wavefunction ψ_L with respect to its reference value ψ_p at τ_p can be obtained by using Eqs. (19, 21-26): [5]

$$\overrightarrow{\psi_L}(\eta)/\psi_p = \mp\frac{E}{6E_D}\left(\left(\left(1 - cos\frac{c}{r_p}\eta\right)^2 + \frac{c^2}{H_\eta^2 a_p^2}\left(\eta - sin\frac{c}{r_p}\eta\right)^2\right)^{1/2}\right) e^{i\cot^{-1}\frac{|H_\eta|a_p\left(1-cos\frac{c}{r_p}\eta\right)}{c\left(\eta - sin\frac{c}{r_p}\eta\right)}} \tag{27}$$

where E/E_D denotes a new dimensionless energy density parameter as the modulus E_D representing the vacuum energy density and the Universe energy density E.

[5] The wavefunction of the space-time continuum could represent the third quantization of the conformal/global gravitational fields, which could be a step towards the quantization of the local relativistic gravitational fields.

Preprints (www.preprints.org) | NOT PEER-REVIEWED | Posted: 21 June 2021 doi:10.20944/preprints202005.0250.v10

4. Evolution of the Universe

The positive and negative solutions of the wavefunction ψ_L imply that matter and antimatter of the plasma evolved in opposite directions. The evolution of the Universe according to the wavefunction for both matter and radiation-only in addition to the light cone are shown in Figure 2a; where only the positive solution of one Universe side is shown due to their symmetry. A chosen mean evolution value of the Hubble parameter of ~70 km·s^{-1}·Mpc^{-1} and a phase transition of expansion at an age of ~10 Gyr were applied to tune the integration constants of the model; the predicted energy density parameter is ~1.16. Further, the Hubble parameter evolution and its rate shown in Figure 2b.

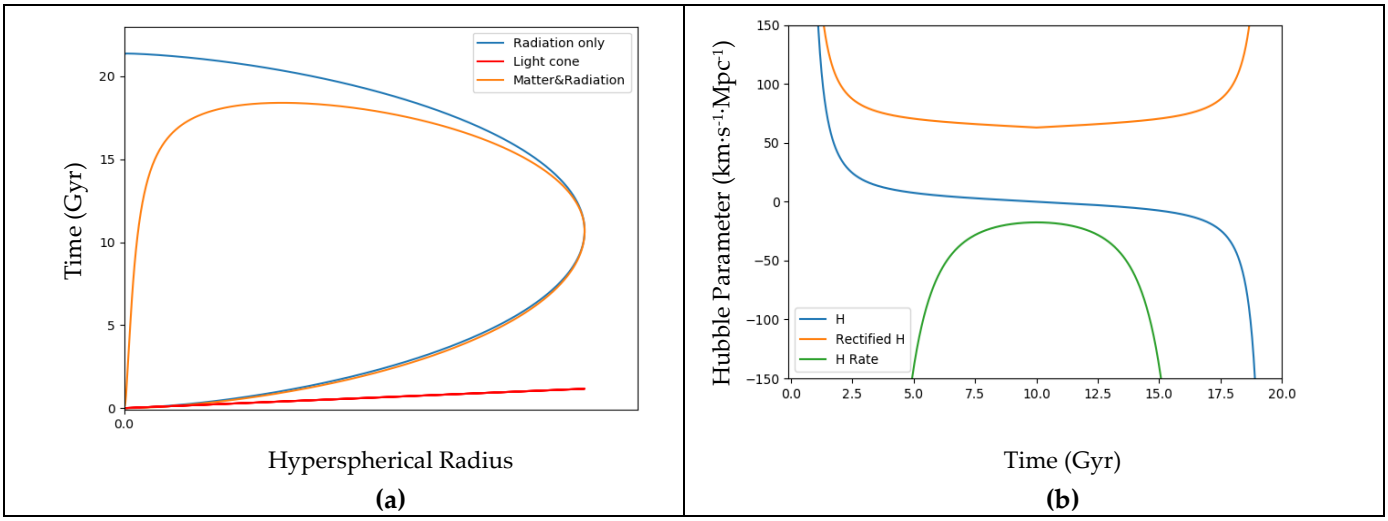

Figure 2. (**a**) Evolution of the wavefunction of matter of one side of the Universe, radiation only wavefunction, in addition to the straight line of light cone (diagram is not to scale). (**b**) The Hubble parameter H evolution and its rate.

According to the matter wavefunction (Figure 2a, orange curve), the cosmic evolution can be interpreted as comprising three distinct phases. Firstly, matter and antimatter sides expand in opposite directions away from early plasma during the first phase perhaps due to the phenomenon of plasma drift in the presence of electromagnetic fields. The expansion speed shown in Figure 2b (blue curve) starts with a hyperbolic rate at the nascent stages, then, the rate decreases due to gravity between the two sides, until it reached its minimal at the phase transition at an age of ~ 10 Gyr. The evolution in the Hubble parameter is evidence from time-delay cosmography and SNe Ia observations [78,79].

However, the matter wavefunction reverses its direction in the second phase with both sides of matter and antimatter entering a state of free-fall towards each other at gravitational acceleration possibly causing current accelerated expansion; the Hubble parameter starts to increase in the reverse direction. According to mechanics, the minus sign of the expansion speed in the second phase (Figure 2b, blue curve) indicates an opposite direction. In addition, the opposite signs of the acceleration (Figure 2b, green curve) and the speed in the first phase indicate a slowing down while the matching signs in the second phase indicate the speed of expansion is increasing.

Interestingly, the matter wavefunction predicts a final phase of spatial contraction that appears after ~18 Gyr, which could be because of the future high concentration of matter/antimatter at both sides that culminates in a Big Crunch, signalling a cyclic Universe. On the other hand, the radiation-only according to its wave function, which propagates faster than matter, is predicted to pass from a side to another side (See Figure 2a, blue curve), which could explain why the CMB can be observed even though matter moves much slower than light. This is could be behind the large-angle correlations of the CMB [80] and the apparent virtualization of the SLOAN Digital Sky Survey data [81].

Preprints (www.preprints.org) | NOT PEER-REVIEWED | Posted: 21 June 2021 doi:10.20944/preprints202005.0250.v10

A congruence of space-time worldlines has been simulated to visualise the matter wavefunction as shown in Figure 3a while the apparent Universe's topology due to the gravitational lensing effects is shown in Figure 3b, possibility matching the large-angle correlations of the CMB [80] and the SLOAN Digital Sky Survey data virtualization [81].

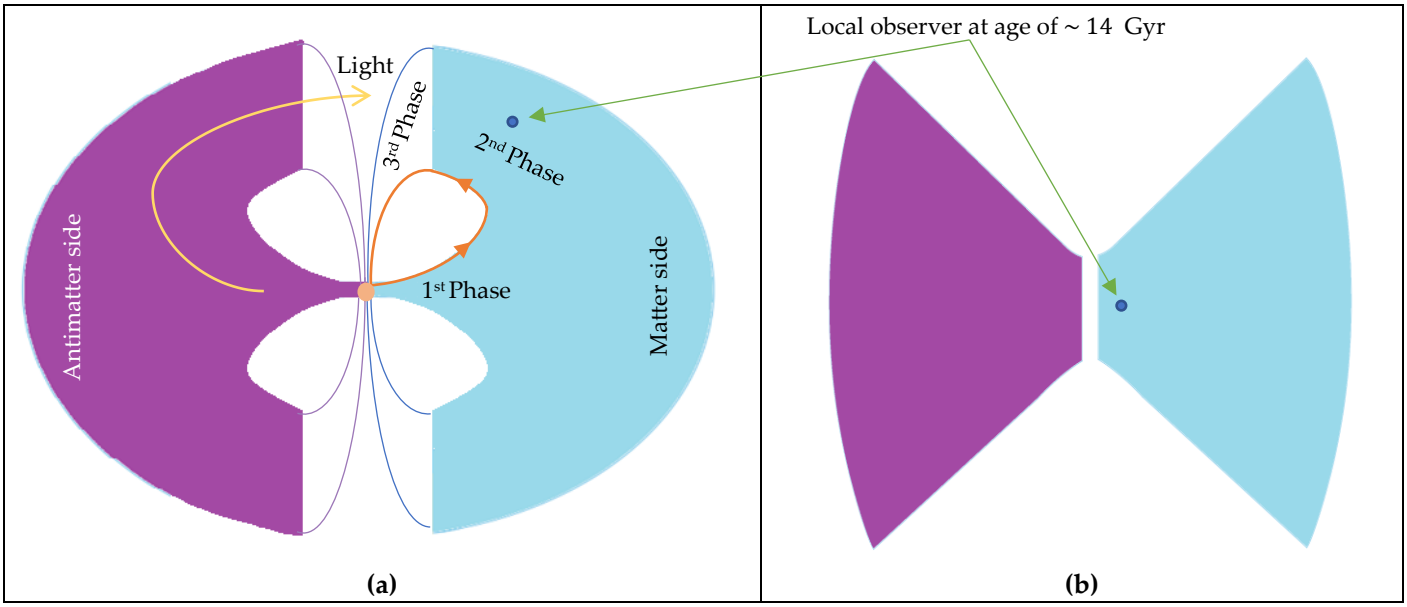

Figure 3. (**a**) A schematic 2D spatial and 1D temporal dimensions of the predicted cosmic topology of both sides where the expansion at the first phase is away from the early plasma while the second phase is corresponding to the reversal of the expansion direction. The future third phase corresponds to a spatial contraction leading to a Big Crunch. (**b**) The apparent topology during the first and second phases caused by the gravitational lensing effects.

Regarding the present space-time flatness, the simulation of the congruence of space-time worldlines coupled with an initial zero or positive curvature has produced a curved geometry in the first phase, which is in agreement with the PL18 release [11,50] where the space-time worldlines are not equal at any age during the first phase as shown in Figure 4a. Conversely, at the present accelerated phase of expansion in the reverse directions, the simulation of the space-time worldlines coupled with initial positive curvature produced equal space-time worldlines or a flat space-time. This is because that the worldlines that propagate the furthest at the first phase, due to initial curvature, will take the longest paths at the second phase due to the reverse directions and vice versa as shown in Figure 4.

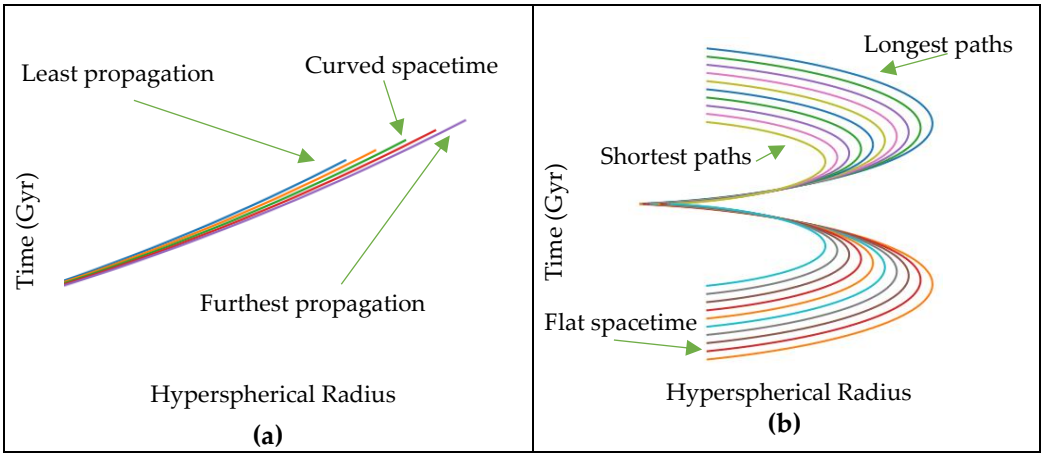

Figure 4. Evolution of space-time worldlines at (**a**) early and **(b)** present Universe.

Preprints (www.preprints.org) | NOT PEER-REVIEWED | Posted: 21 June 2021 doi:10.20944/preprints202005.0250.v10

Since both sides move closer to each other at the second phase; this would increase the average density of the Universe, which can explain the reason for the current increase in the average temperature of the Universe [82] in contrast to the state of cooling down from hot plasma during the first expansion. In addition, the reasoning for current accelerated expansion due to the free-fall of both sides towards each other under gravitational acceleration can also explain the observed dark flow towards the great attractor that cannot be observed [83]. Further, the observed strong "dipole repeller" [84] can endorse this model; the authors argued their observation is incompatible with an attractive gravitational force while the under-dense and over-dense regions explanation for this phenomenon seems incomplete as accordingly, numerous regions which are differently dense would create multiple weak attractors-repellers throughout the Universe. On the other hand, since our local group (Figure 3a, blue dot at age of ~14 Gyr) flows in a direction towards the antimatter side while the corresponding galaxy group in the antimatter side flows in a direction towards our group. Therefore, the flow of the matter side including our group can signify the great attractor while the flow of the antimatter side towards our group can signify the corresponding repeller. Although the matter and antimatter are distinct sides, i.e. no direct collusion, passing of cosmic rays from one side to another would cause spectrum compatible with baryon-antibaryon annihilation, where several antistar candidates were detected by Fermi Large Area Telescope [85,86]. Further, this could explain the origin of the antihelium nuclei by AMS-02 [87].

Figure 5 shows a schematic in 3D spatial and 1D temporal dimensions of the spacetime evolution of both sides of the Universe, which seems to be in correspondence with the Kaluza–Klein unified theory [6]. The cosmic horizon would be as $R(\eta) = \mp\sqrt{c^2t^2 + a^2}$, where t denotes cosmic time.

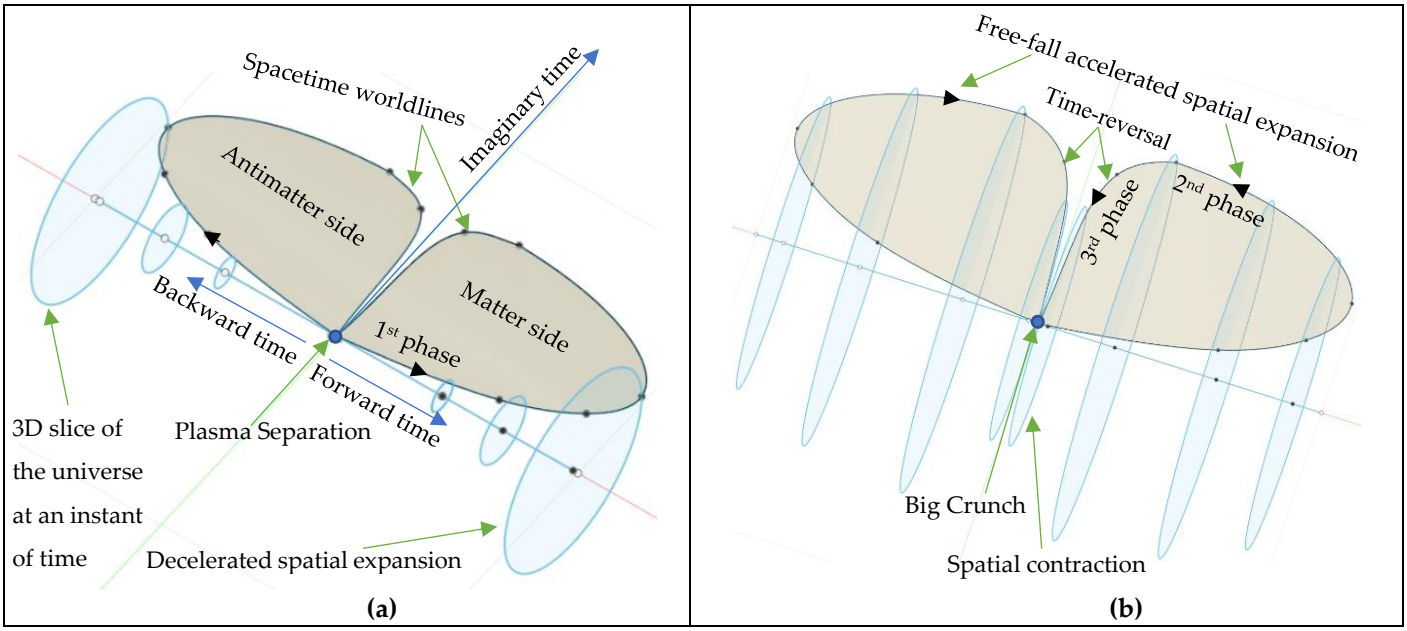

Figure 5. (**a**) A schematic in 3D spatial and 1D temporal dimensions of both sides of the Universe according to the wave function of spacetime worldlines. (**a**) In the first phase, both sides expand away from the early plasma. **(b)** In the second stage, both sides expand in reverse directions and free-fall towards each other at gravitational acceleration. In the third phase, both sides contract leading to the big Crunch. Blue circles represent a 3D slice of the Universe at an instant of time that is not necessarily a simply path connected.

[6] Due to the anisotropy in the expansion of the early Universe hypersphere into two sides, the expansion in time and hence the time dimension can be analyses and considered as two dimensions, the imaginary (future-past) and the real (forward-backwards) time components, where antimatter travels backwards in real time component as employed in Feynman diagrams. Accordingly, the fifth dimension in the Kaluza–Klein theory would be the real-time component while the cylindrical condition would represent the spatial scale factor of each side of the Universe.

Preprints (www.preprints.org) | NOT PEER-REVIEWED | Posted: 21 June 2021 doi:10.20944/preprints202005.0250.v10

5. Galaxy Formation and Rotation in a Reconstructed String Theory Brane Notion

Observations from the DEEP2 Survey of a large sample of disk galaxies found that the motion of galaxies was steadily getting in ordered with their rotation velocity increasing over last eight billion years in contradiction with the previous perception that galaxies are settled with minor changes over that period [88,89]. In addition, galactic rotation curves were found to be influenced by external fields [27] as well as they follow the baryonic Tully-Fisher relation [25,26]. Several studies reported that some galaxies are missing dark matter [90–92] while the Dark Energy Survey Collaboration which released the largest maps of galaxy distribution and shapes showed the dark matter/dark gravity is more distributed than that predicted by the ΛCDM [31,93]. On the other hand, the x-ray emission observations of the G2 cloud orbit have challenged the model of a mere supermassive blackhole at the center of our galaxy which should have destroy it [94,95]; a mere supermassive black hole also arises the blackhole hierarchy problem [96]. Further, observations showed high-energy structures perpendicular on the central plane of disk galaxies [97,98]. These observations challenge dark matter and galaxy formation concepts.

Alternatively, since gravitational forces were stronger when the Universe radius was smaller at the first phase according to Eq. (1), a galaxy could form without the need for dark matter where simulations showed that galaxies can form using modified Newtonian dynamics [99]. The derived model showed the early Universe expanded hyperbolically at nascent stages; thus, a dense super gas cloud that was collapsing while traveling through a curved background/conformal space-time (See Figure 3a) would gain high spinning speed. The high-speed spinning can transform its hyperspherical core (Figure 6a) into almost hypercylindrical shape (Figure 6b). Accordingly, the gravitational contributions come mainly from the extrinsic curvature terms (boundary term) while the intrinsic curvature terms vanish as hypercylinders have no intrinsic curvature [100], thus:

$$\frac{R_{\mu\nu}}{\mathcal{R}} - \frac{1}{2}\frac{R}{\mathcal{R}}g_{\mu\nu} - \frac{R}{\mathcal{R}^2}\mathcal{R}_{\mu\nu} = \frac{T_{\mu\nu}}{E_D} - \frac{R\left(\mathcal{K}_{\mu\nu} - \frac{1}{2}\mathcal{K}\hat{p}_{\mu\nu}\right) - \mathcal{R}\left(K_{\mu\nu} - \frac{1}{2}K\hat{q}_{\mu\nu}\right)}{\mathcal{R}^2} \cong 0 \tag{28}$$

These extended field equations can be utilised to reconstruct the Brane notion to higher dimensions in String theory in form of a local 4D relativistic spacetime (Brane as the dense gas cloud core) of intrinsic curvature $R_{\mu\nu}$ and local boundary $K_{\mu\nu}$, which in turn travels and spins with respect to the independent background (Bulk as the 4D conformal space-time) of intrinsic curvature $\mathcal{R}_{\mu\nu}$ and extrinsic conformal curvature $\mathcal{K}_{\mu\nu}$), of curvature evolving over cosmic time. From Eqs. (29), the intrinsic curvature terms are

$$R_{\mu\nu} = \frac{1}{2}Rg_{\mu\nu} + \frac{R}{\mathcal{R}}\mathcal{R}_{\mu\nu} = \frac{1}{2}R\left(g_{\mu\nu} + 2\tilde{q}_{\mu\nu}\right) \cong 0 \tag{29}$$

where the conformal metric $\tilde{g}_{\mu\nu} = \mathcal{R}_{\mu\nu}/\mathcal{R} = g_{\mu\nu}\Omega^2$. For an ideal case $R_{\mu\nu} = 0$, which results in that the 4D space-time interval is given by the Schwarzschild metric as

$$ds^2 = \left(1 - \frac{{r_s}^2}{r^2}\right)c^2\,dt^2 - \frac{{s_s}^2}{s^2}\left(\frac{dr^2}{1 - \frac{{r_s}^2}{r^2}} + r^2\,d\theta^2 + r^2 sin^2\theta\,d\phi^2\right) \tag{30}$$

where r_s is the Schwarzschild radius. Since the general form of the conformal time is $d\eta = \Omega^2 dt$ and by comparing the conformal transformation of the time coordinate in both Eqs. (30, 31) as $g_{tt} + 2\tilde{q}_{tt} = c^2dt^2 - ({r_s}^2/r^2)c^2dt^2$, which shows the conformal function $\Omega^2 = -{r_s}^2/2r^2$, revealing a spatial shrinking thought conformal time as shown in Figure 6b. This can occur in due to the high spinning. To account for this conformal shrinking, a dimensionless spatial scale factor, ${s_s}^2/s^2$, has been incorporated to the metric in Eq. (30).

Preprints (www.preprints.org) | NOT PEER-REVIEWED | Posted: 21 June 2021 doi:10.20944/preprints202005.0250.v10

The 4D Brane (the gas cloud forming a galaxy) has 4D spin and 4D flow with respect to the 4D Bulk (independent background/conformal space-time) as shown in Figure 6.

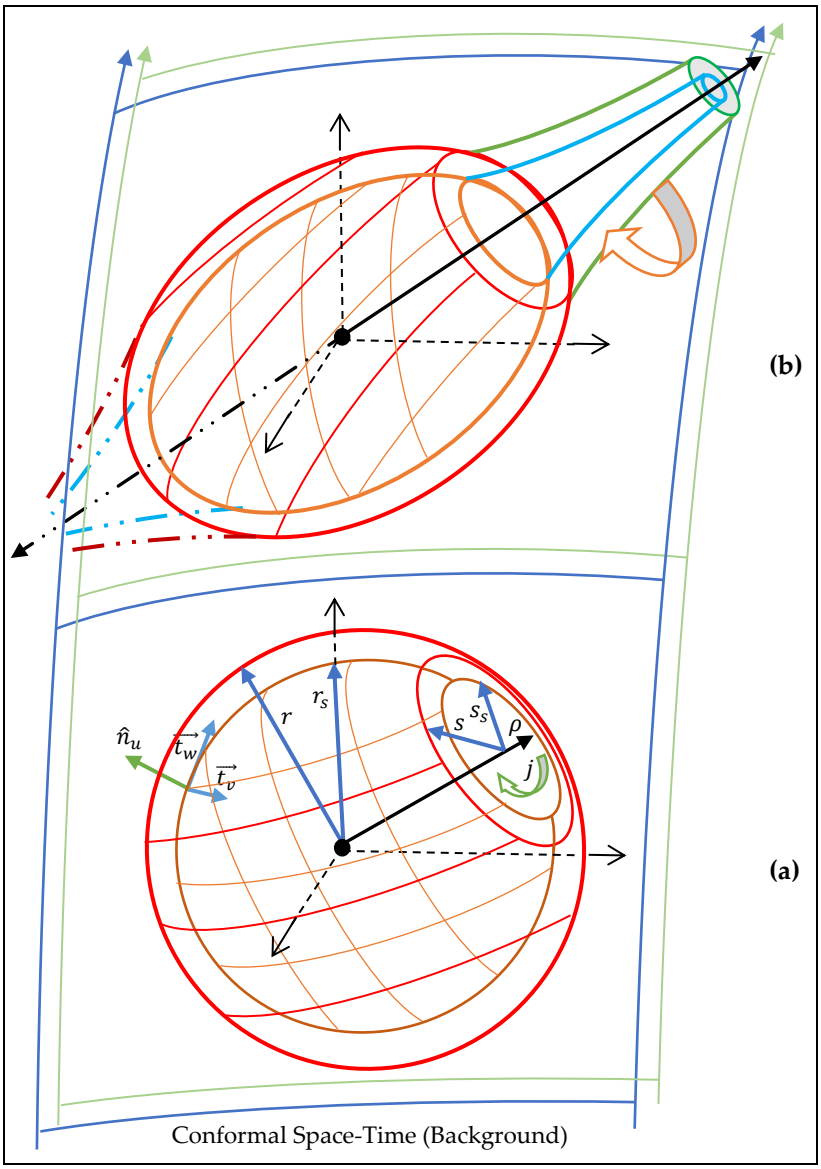

Figure 6. The evolution of the core of a galaxy (the red-orange 4D hypersphere/Brane representing the local relativistic space-time) along its travel and spin through the conformal space-time (the blue-green 4D Bulk representing the independent background of a pre-existing curvature evolving over cosmic time.

However, for a realistic case when $R_{\mu\nu} \cong 0$, the Kerr metric can be utilised to account for the spinning. A dimensionless spatial scale factor, ${s_s}^2/s^2$ is incorporating to account for spatial shrinking through conformal time as

$$ds^2 = \left(1 - \frac{r_s r}{\Sigma}\right) c^2\, dt^2 - \frac{{s_s}^2}{s^2}\left(\frac{\Sigma}{\Delta} dr^2 + \Sigma d\theta^2 + \left(r^2 + a^2 + \frac{r_s r a^2}{\Sigma} sin^2\theta\right) sin^2\theta\, d\phi^2\right) - \frac{2 r_s r a sin^2\theta}{\Sigma} c dt d\phi \quad (31)$$

where $\Sigma = r^2 + a^2 sin^2\theta$ and $\Delta = r^2 - r_s r + a^2$ and $a = J/Mc$; J is the spin momentum.

Preprints (www.preprints.org) | NOT PEER-REVIEWED | Posted: 21 June 2021 doi:10.20944/preprints202005.0250.v10

This scenario of galaxy formation implies that the core of the galaxy forms a central vortex with event horizon as opening leading to opposite traversable wormholes through the conformal time. The galaxy and its core form at the same process while the gas clouds outside the core would form the spiral arms where the fast-rotating core induces frame dragging [101]. The G2 that faced the drag effects should have its orbit around the wormhole but far away from the central mouth. These two opposite wormholes can represent the cosmic filament and explain the possible observational spin evidence of the filament [102]. The formation of supermassive compact cores with a mass of ~10^9 $M_\odot$ at just 6% of current Universe age [103] and the blackhole hierarchy problem could be explained by this scenario. While observed the superluminal motion in the x-ray jet of M87 [1] could be travelling through these traversable wormholes.

To evaluate the influence of the spinning momentum, j, and the curvature of the background on the core of the galaxy (Figure 7a) and the surrounding gas clouds (the spiral arms), a fluid simulation has been performed based on Newtonian dynamics using the Fluid Pressure and Flow software [104]. The conformal curvature of the space-time continuum is predicted to evolve over cosmic time with the highest degree of curvature occurring at the phase transition as determined by the wavefunction (see Figure 3a), thus, in this simulation, the fluid was deemed to represent the space-time continuum throughout incrementally flattening curvature paths representing the conformal curvature evolution. Using these conditions, a fluid model was built to analyse the external momenta exerted on objects flowing throughout the incrementally flattening curvatures. The momenta yielded by the fluid simulation were used to inform a simulation of a spiral galaxy as a forced vortex (under external fields). The simulation shows that the tangential speeds of the outer parts of the spiral galaxy are rotating faster in comparison with the rotational speeds of the inner parts, which is consistent with observations of galaxy rotation.

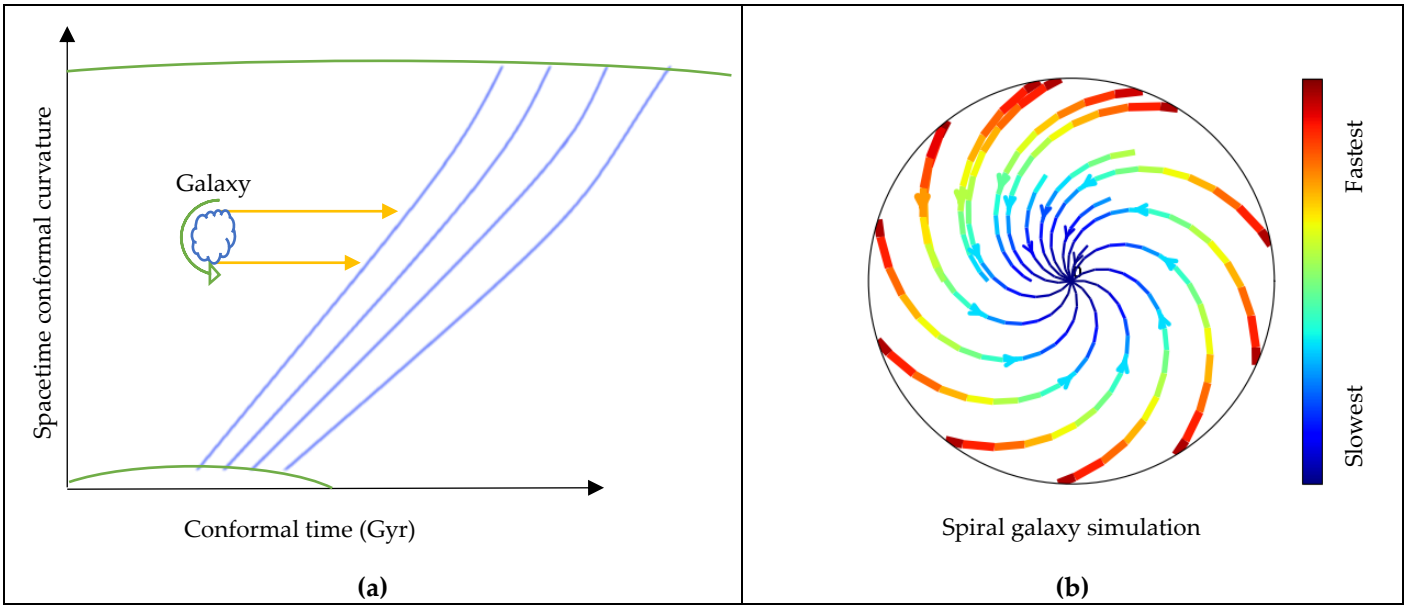

Figure 7. (**a**) External fields exerted on a galaxy due to the space-time conformal curvature evolution. Green curves represent the curvature of space-time worldlines. Blue curves represent the simulated space-time continuum flux. (**b**) Simulation of spiral galaxy rotation. Blue represents the slowest tangential speeds and red represents the fastest speeds.

Accordingly, it can be inferred that the fast orbital speeds observed for outer stars in galaxies are a result of their travel through conformally curved space-time. Since the rotation speed only depends on the galaxy mass and the background curvature, these finding can be consistence with the baryonic Tully-Fisher relation and the detected external fields. The observed galaxies that are missing dark matter could be having travelled through paths of least curved background.

Preprints (www.preprints.org) | NOT PEER-REVIEWED | Posted: 21 June 2021 doi:10.20944/preprints202005.0250.v10

6. Early Universe Boundary Contribution

In case of closed early Universe as hinted by PL18 [11,50,51][11], the gravitational contributions of the early Universe plasma boundary can be obtained by using the boundary term in the extended field equations for high energy limits. At the reference imaginary time τ_p, there is no conformal transformation. Therefore, the global $\mathcal{K}_{\mu\nu}$ and the local $K_{\mu\nu}$ boundaries are the same. Accordingly, the boundary term in the extended field equations reduces to

$$\frac{R-\mathcal{R}}{\mathcal{R}}\left(\mathcal{K}_{\mu\nu}-\frac{1}{2}\mathcal{K}\hat{p}_{\mu\nu}\right)=\frac{8\pi G_t}{c^4}T_{\mu\nu} \tag{32}$$

For smooth hypersphere of early plasma, the induced metric $p_{\mu\nu}$ on its boundary is

$$[p_{\mu\nu}]=diag\left(-c^2,\frac{a^2(t)}{{a_p}^2}R^2,\frac{a^2(t)}{{a_p}^2}R^2sin^2\theta\right), \tag{33}$$

where R is the extrinsic radius of curvature [100]. The extrinsic curvature tensor can be obtained by utilising the formula $\mathcal{K}_{uv}=-\overrightarrow{t_v}.\nabla_u\hat{n}_u$. Due to the smoothness of the hypersphere, the covariant derivative reduces to a partial derivative as $\mathcal{K}_{uv}=-\overrightarrow{t_v}\,\partial\hat{n}_u/\partial\overrightarrow{t^u}$ [100]. The extrinsic curvature tensor at τ_p is

$$[\mathcal{K}_{\mu\nu}]=diag\left(0,-\frac{a^2(t)}{{a_p}^2}R,-\frac{a^2(t)}{{a_p}^2}Rsin^2\theta\right) \tag{34}$$

The trace of the extrinsic curvature is $\mathcal{K}=\mathcal{K}_{\mu\nu}q^{\mu\nu}=2/R$ while the pre-existing/intrinsic curvature of early Universe plasma boundary at τ_p is the Gaussian curvature as $\mathcal{R}_p=1/r_p^2$ [100]. On the other hand, the Ricci scalar curvature R_p at τ_p can be written in terms of the difference between kinetic and potential energy densities whereby substituting Friedmann equations in Eqs. (16-17) into the Ricci scalar curvature in Eq. (15) as

$$R_p=\frac{6G_p}{c^2}\left(\frac{4\pi P_p}{c^2}-\frac{4\pi\rho_p}{3}\right) \tag{35}$$

By solving the boundary term for a perfect fluid given by $T_{\mu\nu}=(\rho+\frac{P}{c^2})\,u_\mu u_\nu+Pg_{\mu\nu}$ [72], and then substituting Eqs. (33-35) into the boundary term in Eq. (32) as

$$\frac{\frac{6G_p}{c^2}\left(\frac{4\pi P_p}{c^2}-\frac{4\pi\rho_p}{3}\right)-\frac{1}{r_p^2}}{1/r_p^2}\left(\frac{-c^2}{r_p^2}\right)=8\pi G_p\rho_p \tag{36}$$

By multiplying both sides by early Universe plasma volume V_p, yields

$$r_p=\frac{4G_p\,P_pV_p}{c^4} \tag{37}$$

The reference radius of curvature $r_p>0$ because any reduction in the early plasma volume causes an increase in its pressure, which can realise a singularity-free paradigm.[7]

[7] The smallest possible reference radius of the early Universe plasma due to its boundary gravitational contributions can reveal that the early Universe expansion upon emission of the CMB could mark the beginning of the Universe from a previous collapsed one. This in agreement with the wavefunction prediction of an eventual time-reversal phase comprising rapid spatial contraction that culminates in a Big Crunch, signalling a cyclic Universe.

 doi:10.20944/preprints202005.0250.v10

7. Conclusions and Future Works

In this study, the pre-existing curvature is incorporated to extend the field equations where a closed early Universe model is considered by utilising a referenced Friedmann–Lemaître metric model incorporating the scale factor of the early Universe and its radius of curvature upon the emission of the CMB. The evolution of the Universe from early plasma is modelled by utilising the Universe wavefunction. The wavefunction revealed both positive and negative solutions implying that the Universe evolved into two opposite sides: matter and antimatter sides.

The derived wavefunction predicted that a nascent hyperbolic expansion away from early plasma is followed by a phase of decelerating spatial expansion during the first ~ 10 Gyr, and then, a second phase of accelerating expansion. The plasma drift in the presence of electromagnetic fields could provide a physical explanation for the expansion of the early Universe against the strong gravitational forces of the early very dense plasma, whereby both sides of the Universe expanded away from the early plasma during the first phase. Then, during the second phase, they reverse their directions and free-fall towards each other. It is conceivable that the matter and antimatter are free-falling towards each other, causing the present accelerating expansion of the Universe. This can explain the effects attributed to dark energy and the observed dark flow while dark energy was found either not constant as the Universe is expanding faster than estimated by ΛCDM or it is not the cause of the accelerated expansion of the Universe [24].

The inverse square law of G_t with respect to the Universe's radius could explain the galaxy formation without involving dark matter where G_t was larger during first phase of expansion. This adds up to the background curvature which enhances galaxy spinning. Regarding the fast-orbital speed of outer stars, the simulation can provide a physical explanation by which the fast orbital speed of outer stars is owing to the external fields exerted on galaxies as they travel through conformally curved space-time rather than the existence of dark matter where dark matter is being challenged by observed external fields that influence galactic rotation speeds. The inverse square law of G_t with respect to the Universe's radius can explain the gravity hierarchy problem.

The simulated space-time worldlines during the decelerating phase were found to be flattened during the accelerating phase due to the reverse direction of the continuum worldlines, explaining the current space-time flatness while at the early Universe, it is showed to be of a positive curvature as hinted by the PL18 release. The radiation only worldlines predicted to pass from one side to another can explain why CMB light can be observed even though matter moves much more slowly than light while the apparent topology is possibly in accordance with the large-angle correlations of the CMB and the SLOAN Digital Sky Survey data.

The wavefunction predicted a final phase of time-reversal of spatial contraction leading to a Big Crunch, signalling a cyclic Universe while the derived smallest possible radius of the early Universe plasma due to its boundary gravitational contributions can reveal that the early Universe expansion upon emission of the CMB could mark the beginning of the Universe from a previous collapse one. Finally, this theoretical work will be tested against observational data in future works.

Acknowledgements: I am very grateful to the Guest Editors of the 1st Electronic Conference on Universe, Prof. Dr. James A. Isenberg, Prof. Dr. Gerald B. Cleaver, Dr. Lijing Shao, Prof. Dr. Gonzalo J. Olmo and Prof. Giacomo Tommei for their support and promotion of the transformative ideas in the full arc of fundamental and interdisciplinary astrophysics research. Special thanks go to the MDPI/Preprints Editors Ms Mila Marinkovic and Ms Bojana Djokic for their rapid and excellent processing of a series of preprints during this work development.

Funding: This research received no funding.

Conflicts of Interest: The author declares no conflict of interest.

Preprints (www.preprints.org) | NOT PEER-REVIEWED | Posted: 21 June 2021 doi:10.20944/preprints202005.0250.v10

Appendix A

The referenced metric and its inverse are

$$g_{\mu\nu} = \begin{pmatrix} c^2 & 0 & 0 & 0 \\ 0 & -\frac{\left(\frac{a^2}{{a_p}^2}\right)}{\left(1-\frac{r^2}{{r_p}^2}\right)} & 0 & 0 \\ 0 & 0 & -\left(\frac{a^2}{{a_p}^2}\right)r^2 & 0 \\ 0 & 0 & 0 & -\left(\frac{a^2}{{a_p}^2}\right)r^2 sin^2\theta \end{pmatrix} \tag{A.1}$$

$$g^{uv} = \begin{pmatrix} \frac{1}{c^2} & 0 & 0 & 0 \\ 0 & -\frac{\left(1-\frac{r^2}{{r_p}^2}\right)}{\left(\frac{a^2}{{a_p}^2}\right)} & 0 & 0 \\ 0 & 0 & \frac{-1}{\left(\frac{a^2}{{a_p}^2}\right)r^2} & 0 \\ 0 & 0 & 0 & \frac{-1}{\left(\frac{a^2}{{a_p}^2}\right)r^2 sin^2\theta} \end{pmatrix} \tag{A.2}$$

The Ricci curvature tensor R_{uv} is solved using the Christoffel symbols of the second kind which is given by $\Gamma^{\rho}_{\mu\nu} = \frac{1}{2}g^{\rho\lambda}(\partial_\mu g_{\lambda\nu} + \partial_\nu g_{\lambda\mu} - \partial_\lambda g_{\mu\nu})$ for the referenced metric tensor $g_{\mu\nu}$. The non-zero Christoffel symbols are:

$$\Gamma^0{}_{11} = \frac{a\dot{a}}{c^2{a_p}^2\left(1-\frac{r^2}{{r_p}^2}\right)} \tag{A.3}$$

$$\Gamma^0{}_{22} = \frac{r^2 a\dot{a}}{c^2{a_p}^2} \tag{A.4}$$

$$\Gamma^0{}_{33} = \frac{r^2 a\dot{a}\, sin^2\theta}{c^2{a_p}^2} \tag{A.5}$$

$$\Gamma^1{}_{11} = \frac{\mathrm{r}}{{r_p}^2\left(1-\frac{r^2}{{r_p}^2}\right)} \tag{A.6}$$

$$\Gamma^1{}_{22} = -\mathrm{r}\left(1-\frac{r^2}{{r_p}^2}\right) \tag{A.7}$$

$$\Gamma^1{}_{33} = -\mathrm{r}sin^2\theta\left(1-\frac{r^2}{{r_p}^2}\right) \tag{A.8}$$

Preprints (www.preprints.org) | NOT PEER-REVIEWED | Posted: 21 June 2021 doi:10.20944/preprints202005.0250.v10

$$\Gamma^1{}_{01} = \Gamma^2{}_{02} = \Gamma^3{}_{03} = \Gamma^1{}_{10} = \Gamma^2{}_{20} = \Gamma^3{}_{30} = \frac{\dot{a}}{a} \tag{A.9}$$

$$\Gamma^2{}_{12} = \Gamma^2{}_{21} = \Gamma^3{}_{13} = \Gamma^3{}_{31} = \frac{1}{r} \tag{A.10}$$

$$\Gamma^2{}_{33} = -sin\,\theta\, cos\theta \tag{A.11}$$

$$\Gamma^3{}_{23} = \Gamma^3{}_{32} = cot\,\theta \tag{A.12}$$

The Ricci curvature tensor given by $R_{\mu\nu} = \partial_\lambda \Gamma^\lambda_{\mu\nu} - \partial_\nu \Gamma^\lambda_{\mu\lambda} + \Gamma^\rho_{\mu\nu}\Gamma^\lambda_{\rho\lambda} - \Gamma^\rho_{\mu\lambda}\Gamma^\lambda_{\rho\nu}$. The non-zero components are solved as follows. The $t-t$ component is

$$R_{tt} = R_{00} = -\partial_0 \Gamma^1{}_{01} - \partial_0 \Gamma^2{}_{02} - \partial_0 \Gamma^3{}_{03} - \Gamma^1{}_{01}\Gamma^1{}_{10} - \Gamma^2{}_{02}\Gamma^2{}_{20} - \Gamma^3{}_{03}\Gamma^3{}_{30} \tag{A.13}$$

$$R_{tt} = -3\partial_t \frac{\dot{a}}{a} - 3\left(\frac{\dot{a}}{a}\right)^2 = -3\frac{\ddot{a}a - \dot{a}^2}{a^2} - 3\frac{\dot{a}^2}{a^2} = -3\frac{\ddot{a}}{a} \tag{A.14}$$

The $r-r$ component of the Ricci tensor is

$$\begin{aligned} R_{rr} = R_{11} = {} & \partial_0 \Gamma^0_{11} - \partial_1 \Gamma^2{}_{12} - \partial_1 \Gamma^3{}_{13} + \Gamma^0{}_{11}\Gamma^2{}_{02} + \Gamma^0{}_{11}\Gamma^3{}_{03} - \Gamma^1{}_{10}\Gamma^0{}_{11} \\ & + \Gamma^1{}_{11}\Gamma^2{}_{12} + \Gamma^1{}_{11}\Gamma^3{}_{13} \end{aligned} \tag{A.15}$$

$$R_{rr} = \partial_t \frac{a\dot{a}}{c^2 {a_p}^2\left(1 - \frac{r^2}{{r_p}^2}\right)} - 2\partial_r \frac{1}{r} + \frac{a\dot{a}}{c^2 {a_p}^2\left(1 - \frac{r^2}{{r_p}^2}\right)}\frac{\dot{a}}{a} + 2\frac{\mathrm{r}}{{r_p}^2\left(1 - \frac{r^2}{{r_p}^2}\right)}\frac{1}{r} - 2\frac{1}{r^2} \tag{A.16}$$

$$R_{rr} = \frac{a\ddot{a}}{c^2 {a_p}^2\left(1 - \frac{r^2}{{r_p}^2}\right)} + \frac{\dot{a}^2}{c^2 {a_p}^2\left(1 - \frac{r^2}{{r_p}^2}\right)} + \frac{\dot{a}^2}{c^2 {a_p}^2\left(1 - \frac{r^2}{{r_p}^2}\right)} + \frac{2}{{r_p}^2\left(1 - \frac{r^2}{{r_p}^2}\right)} \tag{A.17}$$

$$R_{rr} = \frac{\left(\frac{a\ddot{a}}{{a_p}^2} + \frac{2\dot{a}^2}{{a_p}^2} + \frac{2c^2}{{r_p}^2}\right)}{c^2\left(1 - \frac{r^2}{{r_p}^2}\right)} \tag{A.18}$$

The $\theta - \theta$ component is

$$\begin{aligned} R_{\theta\theta} = R_{22} = {} & \partial_0 \Gamma^0{}_{22} + \partial_1 \Gamma^1{}_{22} - \partial_2 \Gamma^3{}_{23} + \Gamma^0{}_{22}\Gamma^1{}_{01} + \Gamma^0{}_{22}\Gamma^3{}_{03} + \Gamma^1{}_{22}\Gamma^1{}_{11} \\ & + \Gamma^1{}_{22}\Gamma^3{}_{13} - \Gamma^2{}_{20}\Gamma^0{}_{22} - \Gamma^2{}_{21}\Gamma^1{}_{22} - \Gamma^3{}_{23}\Gamma^3{}_{32} \end{aligned} \tag{A.19}$$

$$R_{\theta\theta} = \partial_t \frac{r^2 a\dot{a}}{c^2 {a_p}^2} - \partial_r\, \mathrm{r}\left(1 - \frac{r^2}{{r_p}^2}\right) - \partial_\theta \cot(\theta) + \frac{r^2 a\dot{a}}{c^2 {a_p}^2}\frac{\dot{a}}{a} - \mathrm{r}\left(1 - \frac{r^2}{{r_p}^2}\right)\frac{1}{r} - \cot^2(\theta) \tag{A.20}$$

$$R_{\theta\theta} = \frac{r^2 a\ddot{a}}{c^2 {a_p}^2} + \frac{r^2\dot{a}^2}{c^2 {a_p}^2} + \left(3\frac{r^2}{{r_p}^2} - 1\right) + \csc^2(\theta) + \frac{r^2\dot{a}^2}{c^2 {a_p}^2} - \left(1 - \frac{r^2}{{r_p}^2}\right) - \cot^2(\theta) \tag{A.21}$$

Preprints (www.preprints.org) | NOT PEER-REVIEWED | Posted: 21 June 2021 doi:10.20944/preprints202005.0250.v10

$$R_{\theta\theta} = \frac{r^2 a\ddot{a}}{c^2 {a_p}^2} + 2\frac{r^2 \dot{a}^2}{c^2 {a_p}^2} + \left(2\frac{r^2}{{r_p}^2}\right) - 1 + \csc^2(\theta) - \cot^2(\theta) \tag{A.22}$$

$$R_{\theta\theta} = \frac{r^2}{c^2}\left(\frac{a\ddot{a}}{{a_p}^2} + \frac{2\dot{a}^2}{{a_p}^2} + \frac{2c^2}{{r_p}^2}\right) \tag{A.23}$$

The $\phi - \phi$ component is

$$\begin{aligned} R_{\phi\phi} = R_{33} = {} & \partial_0 {\Gamma^0}_{33} + \partial_1 {\Gamma^1}_{33} + \partial_2 {\Gamma^2}_{33} + {\Gamma^0}_{33}{\Gamma^1}_{01} + {\Gamma^0}_{33}{\Gamma^2}_{02} + {\Gamma^1}_{33}{\Gamma^1}_{11} \\ & + {\Gamma^1}_{33}{\Gamma^2}_{12} - {\Gamma^3}_{30}{\Gamma^0}_{33} - {\Gamma^3}_{31}{\Gamma^1}_{33} - {\Gamma^3}_{32}{\Gamma^2}_{33} \end{aligned} \tag{A.24}$$

$$\begin{aligned} R_{\phi\phi} = {} & \partial_t \frac{r^2 a\dot{a}\sin^2\theta}{c^2 {a_p}^2} - \partial_r\, r\sin^2\theta\left(1 - \frac{r^2}{{r_p}^2}\right) - \partial_\theta \sin\theta\cos\theta + 2\frac{r^2 a\dot{a}\sin^2\theta}{c^2 {a_p}^2}\frac{\dot{a}}{a} \\ & - r\sin^2\theta\left(1 - \frac{r^2}{{r_p}^2}\right)\frac{r}{{r_p}^2\left(1 - \frac{r^2}{{r_p}^2}\right)} - r\sin^2\theta\left(1 - \frac{r^2}{{r_p}^2}\right)\frac{1}{r} \\ & - \frac{\dot{a}}{a}\frac{r^2 a\dot{a}\sin^2\theta}{c^2 {a_p}^2} + r\sin^2\theta\left(1 - \frac{r^2}{{r_p}^2}\right)\frac{1}{r} + \sin\theta\cos\theta\cot\theta \end{aligned} \tag{A.25}$$

$$\begin{aligned} R_{\phi\phi} = R_{33} = {} & \frac{r^2 a\ddot{a}\sin^2\theta}{c^2 {a_p}^2} + \frac{r^2\dot{a}^2\sin^2\theta}{c^2 {a_p}^2} - \sin^2\theta\left(1 + 3\frac{r^2}{{r_p}^2}\right) + \sin^2\theta - \cos^2\theta \\ & + \frac{r^2\dot{a}^2\sin^2\theta}{c^2 {a_p}^2} - \sin^2\theta\left(\frac{r^2}{{r_p}^2}\right) + \cos^2\theta \end{aligned} \tag{A.26}$$

$$R_{\phi\phi} = R_{33} = \frac{r^2 a\ddot{a}\sin^2\theta}{c^2 {a_p}^2} + 2\frac{r^2\dot{a}^2\sin^2\theta}{c^2 {a_p}^2} + 2\sin^2\theta\frac{r^2}{{r_p}^2} \tag{A.27}$$

$$R_{\phi\phi} = \frac{r^2\sin^2\theta}{c^2}\left(\frac{a\ddot{a}}{{a_p}^2} + \frac{2\dot{a}^2}{{a_p}^2} + \frac{2c^2}{{r_p}^2}\right) \tag{A.28}$$

Appendix B

This appendix deals with the conformally transformed metric $\hat{g}_{\mu\nu} = g_{\mu\nu} + 2\tilde{q}_{\mu\nu}$. By utilising the conformal time in its parametric form is $d\eta = \frac{a_p}{a}dt$. $\tilde{q}_{\mu\nu} = q_{\mu\nu}\Omega^2$. Thus, the conformally transformed referenced metric and its inverse are

$$\begin{aligned} & \hat{g}_{\mu\nu} = g_{\mu\nu} + 2\tilde{q}_{\mu\nu} \\ & = \begin{pmatrix} \left(1 + 2\frac{a_p}{a}\right)c^2 & 0 & 0 & 0 \\ 0 & -\frac{\left(\frac{a^2}{{a_p}^2}\right)}{\left(1 - \frac{r^2}{{r_p}^2}\right)} & 0 & 0 \\ 0 & 0 & -\left(\frac{a^2}{{a_p}^2}\right)r^2 & 0 \\ 0 & 0 & 0 & -\left(\frac{a^2}{{a_p}^2}\right)r^2\sin^2\theta \end{pmatrix} \end{aligned} \tag{B.1}$$

Preprints (www.preprints.org) | NOT PEER-REVIEWED | Posted: 21 June 2021 doi:10.20944/preprints202005.0250.v10

$$\hat{g}^{uv} = g^{uv} + 2\tilde{q}^{uv}$$

$$= \begin{pmatrix} \frac{1}{\left(1+2\frac{a_p}{a}\right)c^2} & 0 & 0 & 0 \\ 0 & -\frac{\left(1-\frac{r^2}{{r_p}^2}\right)}{\left(\frac{a^2}{{a_p}^2}\right)} & 0 & 0 \\ 0 & 0 & \frac{-1}{\left(\frac{a^2}{{a_p}^2}\right)r^2} & 0 \\ 0 & 0 & 0 & \frac{-1}{\left(\frac{a^2}{{a_p}^2}\right)r^2 sin^2\theta} \end{pmatrix} \quad \text{(B.2)}$$

The non-zero Christoffel symbols are:

$$\Gamma^0{}_{00} = -\frac{\dot{a}}{a}\left(\frac{a_p}{a+2a_p}\right) \quad \text{(B.3)}$$

$$\Gamma^0{}_{11} = \frac{a\dot{a}}{c^2{a_p}^2\left(1-\frac{r^2}{{r_p}^2}\right)}\left(\frac{a}{a+2a_p}\right) \quad \text{(B.4)}$$

$$\Gamma^0{}_{22} = \frac{r^2 a\dot{a}}{c^2{a_p}^2}\left(\frac{a}{a+2a_p}\right) \quad \text{(B.5)}$$

$$\Gamma^0{}_{33} = \frac{r^2 a\dot{a}\, sin^2\theta}{c^2{a_p}^2}\left(\frac{a}{a+2a_p}\right) \quad \text{(B.6)}$$

$$\Gamma^1{}_{11} = \frac{\mathrm{r}}{{r_p}^2\left(1-\frac{r^2}{{r_p}^2}\right)} \quad \text{(B.7)}$$

$$\Gamma^1{}_{22} = -\mathrm{r}\left(1-\frac{r^2}{{r_p}^2}\right) \quad \text{(B.8)}$$

$$\Gamma^1{}_{33} = -\mathrm{r}sin^2\theta\left(1-\frac{r^2}{{r_p}^2}\right) \quad \text{(B.9)}$$

$$\Gamma^1{}_{01} = \Gamma^2{}_{02} = \Gamma^3{}_{03} = \Gamma^1{}_{10} = \Gamma^2{}_{20} = \Gamma^3{}_{30} = \frac{\dot{a}}{a} \quad \text{(B.10)}$$

$$\Gamma^2{}_{12} = \Gamma^2{}_{21} = \Gamma^3{}_{13} = \Gamma^3{}_{31} = \frac{1}{r} \quad \text{(B.11)}$$

$$\Gamma^2{}_{33} = -sin\,\theta\, cos\theta \quad \text{(B.12)}$$

$$\Gamma^3{}_{23} = \Gamma^3{}_{32} = cot\,\theta \quad \text{(B.13)}$$

Preprints (www.preprints.org) | NOT PEER-REVIEWED | Posted: 21 June 2021 doi:10.20944/preprints202005.0250.v10

Appendix C

This appendix deals with the conformally transformed metric tensor $\hat{g}_{\mu\nu} = g_{\mu\nu} + 2\tilde{q}_{\mu\nu}$ of both spatial and temporal coordinates, where the conformally transformed referenced metric tensor and its inverse are

$\hat{g}_{\mu\nu} = g_{\mu\nu} + 2\tilde{q}_{\mu\nu} =$

$$\begin{pmatrix} \left(1+2\frac{a_p}{\mathrm{a}}\right)c^2 & 0 & 0 & 0 \\ 0 & -\frac{\left(\frac{a^2}{{a_p}^2}+2\frac{\mathrm{a}}{a_p}\right)}{\left(1-\frac{r^2}{{r_p}^2}\right)} & 0 & 0 \\ 0 & 0 & -\left(\frac{a^2}{{a_p}^2}+2\frac{\mathrm{a}}{a_p}\right)r^2 & 0 \\ 0 & 0 & 0 & -\left(\frac{a^2}{{a_p}^2}+2\frac{\mathrm{a}}{a_p}\right)r^2 sin^2\theta \end{pmatrix} \quad \text{(C.1)}$$

$$\hat{g}^{uv} = g^{uv} + 2\tilde{q}^{uv}$$

$$= \begin{pmatrix} \frac{1}{\left(1+2\frac{a_p}{\mathrm{a}}\right)c^2} & 0 & 0 & 0 \\ 0 & -\frac{\left(1-\frac{r^2}{{r_p}^2}\right)}{\left(\frac{a^2}{{a_p}^2}+2\frac{\mathrm{a}}{a_p}\right)} & 0 & 0 \\ 0 & 0 & \frac{-1}{\left(\frac{a^2}{{a_p}^2}+2\frac{\mathrm{a}}{a_p}\right)r^2} & 0 \\ 0 & 0 & 0 & \frac{-1}{\left(\frac{a^2}{{a_p}^2}+2\frac{\mathrm{a}}{a_p}\right)r^2 sin^2\theta} \end{pmatrix} \quad \text{(C.2)}$$

The non-zero Christoffel symbols are:

$$\Gamma^0{}_{00} = -\frac{\dot{a}}{a}\frac{a_p}{(a+2a_p)} \quad \text{(C.3)}$$

$$\Gamma^0{}_{11} = \frac{a\dot{a}}{c^2{a_p}^2\left(1-\frac{r^2}{{r_p}^2}\right)}\frac{(a+a_p)}{(a+2a_p)} \quad \text{(C.4)}$$

$$\Gamma^0{}_{22} = \frac{r^2 a\dot{a}}{c^2{a_p}^2}\frac{(a+a_p)}{(a+2a_p)} \quad \text{(C.5)}$$

$$\Gamma^0{}_{33} = \frac{r^2 a\dot{a}\,sin^2\theta}{c^2{a_p}^2}\frac{(a+a_p)}{(a+2a_p)} \quad \text{(C.6)}$$

$$\Gamma^1{}_{11} = \frac{\mathrm{r}}{{r_p}^2\left(1-\frac{r^2}{{r_p}^2}\right)} \quad \text{(C.7)}$$

 doi:10.20944/preprints202005.0250.v10

$$\Gamma^1{}_{22} = -\mathrm{r}\left(1 - \frac{r^2}{{r_p}^2}\right) \tag{C.8}$$

$$\Gamma^1{}_{33} = -\mathrm{r}sin^2\theta\left(1 - \frac{r^2}{{r_p}^2}\right) \tag{C.9}$$

$$\Gamma^1{}_{01} = \Gamma^2{}_{02} = \Gamma^3{}_{03} = \Gamma^1{}_{10} = \Gamma^2{}_{20} = \Gamma^3{}_{30} = \frac{\dot{a}}{a}\frac{(a + a_p)}{(a + 2a_p)} \tag{C.10}$$

$$\Gamma^2{}_{12} = \Gamma^2{}_{21} = \Gamma^3{}_{13} = \Gamma^3{}_{31} = \frac{1}{r} \tag{C.11}$$

$$\Gamma^2{}_{33} = -sin\,\theta\,cos\theta \tag{C.12}$$

$$\Gamma^3{}_{23} = \Gamma^3{}_{32} = cot\,\theta \tag{C.13}$$

References

[1] Planck Collaboration, Akrami Y, Ashdown M, Aumont J, Baccigalupi C, Ballardini M, Banday A J, Barreiro R B, Bartolo N, Basak S, Benabed K, Bersanelli M, Bielewicz P, Bock J J, Bond J R, Borrill J, Bouchet F R, Boulanger F, Bucher M, Burigana C, Butler R C, Calabrese E, Cardoso J-F, Casaponsa B, Chiang H C, Colombo L P L, Combet C, Contreras D, Crill B P, de Bernardis P, de Zotti G, Delabrouille J, Delouis J-M, Di Valentino E, Diego J M, Doré O, Douspis M, Ducout A, Dupac X, Efstathiou G, Elsner F, Enßlin T A, Eriksen H K, Fantaye Y, Fernandez-Cobos R, Finelli F, Frailis M, Fraisse A A, Franceschi E, Frolov A, Galeotta S, Galli S, Ganga K, Génova-Santos R T, Gerbino M, Ghosh T, González-Nuevo J, Górski K M, Gruppuso A, Gudmundsson J E, Hamann J, Handley W, Hansen F K, Herranz D, Hivon E, Huang Z, Jaffe A H, Jones W C, Keihänen E, Keskitalo R, Kiiveri K, Kim J, Krachmalnicoff N, Kunz M, Kurki-Suonio H, Lagache G, Lamarre J-M, Lasenby A, Lattanzi M, Lawrence C R, Jeune M Le, Levrier F, Liguori M, Lilje P B, Lindholm V, López-Caniego M, Ma Y-Z, Macías-Pérez J F, Maggio G, Maino D, Mandolesi N, Mangilli A, Marcos-Caballero A, Maris M, Martin P G, Martínez-González E, Matarrese S, Mauri N, et al 2019 Planck 2018 results. VII. Isotropy and Statistics of the CMB *Astron. Astrophys.* **641** 24

[2] Alpher R A, Bethe H and Gamow G 1948 The origin of chemical elements [1] *Phys. Rev.* **73** 803–4

[3] Wu C S, Ambler E, Hayward R W, Hoppes D D and Hudson R P 1957 Experimental test of parity conservation in beta decay [5] *Phys. Rev.* **105** 1413–5

[4] Canetti L, Drewes M and Shaposhnikov M 2012 Matter and antimatter in the universe *New J. Phys.* **14**

[5] Ahmadi M, Alves B X R, Baker C J, Bertsche W, Capra A, Carruth C, Cesar C L, Charlton M, Cohen S, Collister R, Eriksson S, Evans A, Evetts N, Fajans J, Friesen T, Fujiwara M C, Gill D R, Granum P, Hangst J S, Hardy W N, Hayden M E, Hunter E D, Isaac C A, Johnson M A, Jones J M, Jones S A, Jonsell S, Khramov A, Knapp P, Kurchaninov L, Madsen N, Maxwell D, McKenna J T K, Menary S, Michan J M, Momose T, Munich J J, Olchanski K, Olin A, Pusa P, Rasmussen C, Robicheaux F, Sacramento R L, Sameed M, Sarid E, Silveira D M, So C, Starko D M, Stutter G, Tharp T D, Thompson R I, van der Werf D P and Wurtele J S 2020 Investigation of the fine structure of antihydrogen *Nature* **578** 375–80

[6] Ahmadi M, Alves B X R, Baker C J, Bertsche W, Capra A, Carruth C, Cesar C L, Charlton M, Cohen S, Collister R, Eriksson S, Evans A, Evetts N, Fajans J, Friesen T, Fujiwara M C, Gill D R, Hangst J S, Hardy W N, Hayden M E, Isaac C A, Johnson M A, Jones J M, Jones S A, Jonsell S, Khramov A, Knapp P, Kurchaninov L, Madsen N, Maxwell D, McKenna J T K, Menary S, Momose T, Munich J J, Olchanski K, Olin A, Pusa P, Rasmussen C, Robicheaux F, Sacramento R L, Sameed M, Sarid E, Silveira D M, Stutter G, So C, Tharp T D, Thompson R I, Van Der Werf D P and Wurtele J S 2018 Characterization of the 1S-

2S transition in antihydrogen *Nature* **557** 71–5

[7] Minami Y and Komatsu E 2020 New Extraction of the Cosmic Birefringence from the Planck 2018 Polarization Data *Phys. Rev. Lett.* **125** 221301

[8] Subramanian K 2015 The origin, evolution and signatures of primordial magnetic fields *Reports Prog. Phys.* **79**

[9] Furlanetto S R and Loeb A 2001 *INTERGALACTIC MAGNETIC FIELDS FROM QUASAR OUTFLOWS* vol 556

[10] Bertone S, Vogt C and Enßlin T 2006 Magnetic field seeding by galactic winds *Mon. Not. R. Astron. Soc* **370** 319–30

[11] Di Valentino E, Melchiorri A and Silk J 2020 Planck evidence for a closed Universe and a possible crisis for cosmology *Nat. Astron.* **4** 196–203

[12] Klein O 1966 Instead of cosmology *Nature* **211** 1337–41

[13] Klein O 1971 Arguments concerning relativity and cosmology *Science (80-.).* **171** 339–45

[14] Riess A G 2020 The expansion of the Universe is faster than expected *Nat. Rev. Phys.* **2** 10–2

[15] Riess A G, Casertano S, Yuan W, Macri L M and Scolnic D 2019 Large magellanic cloud cepheid standards provide a 1% foundation for the determination of the hubble constant and stronger evidence for physics beyond ΛCDM *arXiv* **876** 85

[16] Riess A G, Filippenko A V., Challis P, Clocchiatti A, Diercks A, Garnavich P M, Gilliland R L, Hogan C J, Jha S, Kirshner R P, Leibundgut B, Phillips M M, Reiss D, Schmidt B P, Schommer R A, Smith R C, Spyromilio J, Stubbs C, Suntzeff N B and Tonry J 1998 Observational Evidence from Supernovae for an Accelerating Universe and a Cosmological Constant *Astron. J.* **116** 1009–38

[17] Riess A G, Casertano S, Yuan W, Macri L, Anderson J, Mackenty J W, Bowers J B, Clubb K I, Filippenko A V., Jones D O and Tucker B E 2018 New Parallaxes of Galactic Cepheids from Spatially Scanning the Hubble Space Telescope: Implications for the Hubble Constant *Astrophys. J.* **855** 136

[18] Camarena D and Marra V 2020 Local determination of the Hubble constant and the deceleration parameter *Phys. Rev. Res.* **2** 013028

[19] Wong K C, Suyu S H, C-F Chen G, Rusu C E, Millon M, Sluse D, Bonvin V, Fassnacht C D, Taubenberger S, Auger M W, Birrer S, H Chan J H, Courbin F, Hilbert S, Tihhonova O, Treu T, Agnello A, Ding X, Jee I, Komatsu E, Shajib A J, Sonnenfeld A, Blandford R D, E Koopmans L V, Marshall P J and Meylan G 2020 H0LiCOW-XIII. A 2.4 per cent measurement of H 0 from lensed quasars: 5.3σ tension between early-and late-Universe probes *MNRAS* **498** 1420–39

[20] Adler R J, Casey B and Jacob O C 1995 Vacuum catastrophe: An elementary exposition of the cosmological constant problem *Am. J. Phys.* **63** 620–6

[21] Sahni V 2002 The Cosmological Constant Problem and Quintessence *Class. Quantum Gravity* **19** 3435–48

[22] Stainhardt P J and Turok N 2006 Why the cosmological constant is small and positive *Science (80-.).* **312** 1180–3

[23] Rugh S E and Zinkernagel H 2000 The Quantum Vacuum and the Cosmological Constant Problem *Stud. Hist. Philos. Sci. Part B - Stud. Hist. Philos. Mod. Phys.* **33** 663–705

[24] Ryskin G 2020 Vanishing vacuum energy *Astropart. Phys.* **115** 102387

[25] Kroupa P 2012 The dark matter crisis: Falsification of the current standard model of cosmology *Publ. Astron. Soc. Aust.* **29** 395–433

[26] McGaugh S S 2012 The baryonic tully-fisher relation of gas-rich galaxies as a test of ΛcDM and MOND *Astron. J.* **143** 40

[27] Chae K H, Lelli F, Desmond H, McGaugh S S, Li P and Schombert J M 2020 Testing the strong equivalence principle: Detection of the external field effect in rotationally supported galaxies *arXiv* **904** 51

[28] Hildebrandt H, Viola M, Heymans C, Joudaki S, Kuijken K, Blake C, Erben T, Joachimi B, Klaes D, Miller L, Morrison C B, Nakajima R, Verdoes Kleijn G, Amon A, Choi A, Covone G, de Jong J T A, Dvornik A, Fenech Conti I, Grado A, Harnois-Déraps J, Herbonnet R, Hoekstra H, Köhlinger F, McFarland J, Mead A, Merten J, Napolitano N, Peacock J A, Radovich M, Schneider P, Simon P, Valentijn E A, van den Busch J L, van Uitert E and Van Waerbeke L 2017 KiDS-450: Cosmological

parameter constraints from tomographic weak gravitational lensing *Mon. Not. R. Astron. Soc.* **465** 1–50

[29] Gannouji R, Kazantzidis L, Perivolaropoulos L and Polarski D 2018 *Consistency of Modified Gravity with a decreasing G eff (z) in a ΛCDM background*

[30] Saridakis E N, Lazkoz R, Salzano V, Moniz P V, Capozziello S, Jiménez J B, De Laurentis M, Olmo G J, Akrami Y, Bahamonde S, Blázquez-Salcedo J L, Böhmer C G, Bonvin C, Bouhmadi-López M, Brax P, Calcagni G, Casadio R, Cembranos J A R, de la Cruz-Dombriz Á, Davis A-C, Delhom A, Di Valentino E, Dialektopoulos K F, Elder B, Ezquiaga J M, Frusciante N, Garattini R, Gergely L Á, Giusti A, Heisenberg L, Hohmann M, Iosifidis D, Kazantzidis L, Kleihaus B, Koivisto T S, Kunz J, Lobo F S N, Martinelli M, Martín-Moruno P, Mimoso J P, Mota D F, Peirone S, Perivolaropoulos L, Pettorino V, Pfeifer C, Pizzuti L, Rubiera-Garcia D, Said J L, Sakellariadou M, Saltas I D, Mancini A S, Voicu N and Wojnar A 2021 Modified Gravity and Cosmology: An Update by the CANTATA Network *Konstantinos F. Dialektopoulos* **12** 25

[31] Amon A, Gruen D, Troxel M A, MacCrann N, Dodelson S, Choi A, Doux C, Secco L F, Samuroff S, Krause E, Cordero J, Myles J, DeRose J, Wechsler R H, Gatti M, Navarro-Alsina A, Bernstein G M, Jain B, Blazek J, Alarcon A, Ferté A, Raveri M, Lemos P, Campos A, Prat J, Sánchez C, Jarvis M, Alves O, Andrade-Oliveira F, Baxter E, Bechtol K, Becker M R, Bridle S L, Camacho H, Campos A, Rosell A C, Kind M C, Cawthon R, Chang C, Chen R, Chintalapati P, Crocce M, Davis C, Diehl H T, Drlica-Wagner A, Eckert K, Eifler T F, Elvin-Poole J, Everett S, Fang X, Fosalba P, Friedrich O, Giannini G, Gruendl R A, Harrison I, Hartley W G, Herner K, Huang H, Huff E M, Huterer D, Kuropatkin N, Leget P-F, Liddle A R, McCullough J, Muir J, Pandey S, Park Y, Porredon A, Refregier A, Rollins R P, Roodman A, Rosenfeld R, Ross A J, Rykoff E S, Sanchez J, Sevilla-Noarbe I, Sheldon E, Shin T, Troja A, Tutusaus I, Varga T N, Weaverdyck N, Yanny B, Yin B, Zhang Y, Zuntz J, Aguena M, Allam S, Annis J, Bacon D, Bertin E, Bhargava S, Brooks D, Buckley-Geer E, Burke D L, Carretero J, Costanzi M, da Costa L N, et al 2021 Dark Energy Survey Year 3 Results: Cosmology from Cosmic Shear and Robustness to Data Calibration **21** 68

[32] Maeder A 2017 An alternative to the LCDM model: the case of scale invariance *Astrophys. J.* **834** 194

[33] Brouwer M M, Visser M R, Dvornik A, Hoekstra H, Kuijken K, Valentijn E A, Bilicki M, Blake C, Brough S, Buddelmeijer H, Erben T, Heymans C, Hildebrandt H, Holwerda B W, Hopkins A M, Klaes D, Liske J, Loveday J, McFarland J, Nakajima R, Sifón C and Taylor E N 2016 First test of Verlinde's theory of Emergent Gravity using Weak Gravitational Lensing measurements *Mon. Not. R. Astron. Soc.* **466** 2547–59

[34] Chadwick E A, Hodgkinson T F and McDonald G S 2013 Gravitational theoretical development supporting MOND *Phys. Rev. D - Part. Fields, Gravit. Cosmol.* **88** 024036

[35] Van Meter J R 2018 Dark-matter-like solutions to Einstein's unified field equations *Phys. Rev. D* **97** 044018

[36] Milgrom M 2019 MOND in galaxy groups: A superior sample *Phys. Rev. D* **99** 044041

[37] Sofue Y and Rubin V 2000 Rotation Curves of Spiral Galaxies *Annu. Rev. Astron. Astrophys.* **39** 137–74

[38] Clowe D, Gonzalez A and Markevitch M 2003 Weak lensing mass reconstruction of the interacting cluster 1E0657-558: Direct evidence for the existence of dark matter *Astrophys. J.* **604** 596–603

[39] Markevitch M, Gonzalez A H, Clowe D, Vikhlinin A, David L, Forman W, Jones C, Murray S and Tucker W 2003 Direct constraints on the dark matter self-interaction cross-section from the merging galaxy cluster 1E0657-56 *Astrophys. J.* **606** 819–24

[40] X-ray Observatory C *Bullet Cluster: Direct Proof of Dark Matter*

[41] Albert Robson B 2019 Introductory Chapter: Standard Model of Cosmology *Redefining Standard Model Cosmology* (IntechOpen)

[42] Wilczynska M R, Webb J K, Bainbridge M, Barrow J D, Bosman S E I, Carswell R F, Dąbrowski M P, Dumont V, Lee C C, Leite A C, Leszczyńska K, Liske J, Marosek K, Martins C J A P, Milaković D, Molaro P and Pasquini L 2020 Four direct measurements of the fine-structure constant 13 billion years ago *Sci. Adv.* **6** eaay9672

[43] Singal A K 2021 Our Peculiar Motion Inferred from Number Counts of Mid Infra Red AGNs and the Discordance Seen with the Cosmological Principle *Universe* **7** 107

[44] Migkas K, Schellenberger G, Reiprich T H, Pacaud F, Ramos-Ceja M E and Lovisari L 2020 Probing cosmic isotropy with a new X-ray galaxy cluster sample through the L X- T scaling relation *Astron. Astrophys.* **636** 15

[45] Reiprich ; and Aifa T H (*Mapping the X-ray Sky with SRG: First Results from eROSITA and ART-XC*

[46] Schwarz D J, Copi C J, Huterer D and Starkman G D 2015 CMB Anomalies after Planck *Class. Quantum Gravity* **33**

[47] Cuceu A, Farr J, Lemos P and Font-Ribera A 2019 Baryon Acoustic Oscillations and the Hubble Constant: Past, Present and Future *J. Cosmol. Astropart. Phys.* **2019**

[48] Evslin J 2017 Isolating the Lyman alpha forest BAO anomaly *J. Cosmol. Astropart. Phys.* **2017** 024

[49] Asencio E, Banik I and Kroupa P 2021 A massive blow for ΛCDM - The high redshift, mass, and collision velocity of the interacting galaxy cluster El Gordo contradicts concordance cosmology *Mon. Not. R. Astron. Soc.* **500** 5249–67

[50] Handley W 2021 Curvature tension: Evidence for a closed universe *Phys. Rev. D* **103** L041301

[51] Aghanim N, Akrami Y, Ashdown M, Aumont J, Baccigalupi C, Ballardini M, Banday A J, Barreiro R B, Bartolo N, Basak S, Battye R, Benabed K, Bernard J P, Bersanelli M, Bielewicz P, Bock J J, Bond J R, Borrill J, Bouchet F R, Boulanger F, Bucher M, Burigana C, Butler R C, Calabrese E, Cardoso J F, Carron J, Challinor A, Chiang H C, Chluba J, Colombo L P L, Combet C, Contreras D, Crill B P, Cuttaia F, De Bernardis P, De Zotti G, Delabrouille J, Delouis J M, Di Valentino E, Diego J M, Doré O, Douspis M, Ducout A, Dupac X, Dusini S, Efstathiou G, Elsner F, Enßlin T A, Eriksen H K, Fantaye Y, Farhang M, Fergusson J, Fernandez-Cobos R, Finelli F, Forastieri F, Frailis M, Fraisse A A, Franceschi E, Frolov A, Galeotta S, Galli S, Ganga K, Génova-Santos R T, Gerbino M, Ghosh T, González-Nuevo J, Górski K M, Gratton S, Gruppuso A, Gudmundsson J E, Hamann J, Handley W, Hansen F K, Herranz D, Hildebrandt S R, Hivon E, Huang Z, Jaffe A H, Jones W C, Karakci A, Keihänen E, Keskitalo R, Kiiveri K, Kim J, Kisner T S, Knox L, Krachmalnicoff N, Kunz M, Kurki-Suonio H, Lagache G, Lamarre J M, Lasenby A, Lattanzi M, Lawrence C R, Le Jeune M, Lemos P, Lesgourgues J, Levrier F, et al 2020 Planck 2018 results: VI. Cosmological parameters *Astron. Astrophys.* **641**

[52] Meneghetti M, Davoli G, Bergamini P, Rosati P, Natarajan P, Giocoli C, Caminha G B, Metcalf R B, Rasia E, Borgani S, Calura F, Grillo C, Mercurio A and Vanzella E 2020 An excess of small-scale gravitational lenses observed in galaxy clusters *Science (80-.).* **369** 1347–51

[53] Umetsu K 2020 Cluster–galaxy weak lensing *Astron. Astrophys. Rev.* **28** 1–106

[54] Lusso E, Piedipalumbo E, Risaliti G, Paolillo M, Bisogni S, Nardini E and Amati L 2019 Tension with the flat {\Lambda}CDM model from a high redshift Hubble Diagram of supernovae, quasars and gamma-ray bursts *Astron. Astrophys.* **628**

[55] Berti E, Barausse E, Cardoso V, Gualtieri L, Pani P, Sperhake U, Stein L C, Wex N, Yagi K, Baker T, Burgess C P, Coelho F S, Doneva D, De Felice A, Ferreira P G, Freire P C C, Healy J, Herdeiro C, Horbatsch M, Kleihaus B, Klein A, Kokkotas K, Kunz J, Laguna P, Lang R N, Li T G F, Littenberg T, Matas A, Mirshekari S, Okawa H, Radu E, O'Shaughnessy R, Sathyaprakash B S, Van Den Broeck C, Winther H A, Witek H, Aghili M E, Alsing J, Bolen B, Bombelli L, Caudill S, Chen L, Degollado J C, Fujita R, Gao C, Gerosa D, Kamali S, Silva H O, Rosa J G, Sadeghian L, Sampaio M, Sotani H and Zilhao M 2015 Testing general relativity with present and future astrophysical observations *Class. Quantum Gravity* **32**

[56] Debono I and Smoot G F 2016 General relativity and cosmology: Unsolved questions and future directions *Universe* **2** 23

[57] Roger Penrose 2004 *The Road to Reality, Sir Roger Penrose*

[58] Efstathiou G 2003 *Is the low cosmic microwave background quadrupole a signature of spatial curvature?* vol 343

[59] Al-Fadhli M B 2020 On Spacetime Duality and Bounce Cosmology of a Dual Universe *Prepr. 10.20944/preprints202005.0250.v7*

[60] Landau L D 1986 *Theory of Elasticity* (Elsevier)

[61] Dirac P A M 1938 A new basis for cosmology *Proc. R. Soc. A Math. Phys. Eng. Sci.* **165** 199–208

[62] Sobral D, Smail I, Best P N, Geach J E, Matsuda Y, Stott J P, Cirasuolo M and Kurk J 2012 *A large Hα survey at z = 2.23, 1.47, 0.84 & 0.40: the 11 Gyr evolution of star-forming galaxies from HiZELS* vol 000

[63] Quinn T, Parks H, Speake C and Davis R 2013 Improved determination of G using two methods *Phys. Rev. Lett.* **111** 101102

[64] Donoghue J F 2003 Spatial and temporal gradients in the cosmological constant *J. High Energy Phys.* **7** 1115–29

[65] Uzan J P 2011 Varying constants, gravitation and cosmology *Living Rev. Relativ.* **14** 1–155

[66] Gómez-Valent A 2017 *VACUUM ENERGY IN QUANTUM FIELD THEORY AND COSMOLOGY*

[67] S. M. Carroll 2003 Spacetime and Geometry: An Introduction to General Relativity

[68] Dyer E and Hinterbichler K 2009 Boundary terms, variational principles, and higher derivative modified gravity *Phys. Rev. D - Part. Fields, Gravit. Cosmol.* **79**

[69] Guarnizo A, Castañeda L and Tejeiro J M 2010 Boundary term in metric f (R) gravity: field equations in the metric formalism *Gen Relativ Gravit* **42** 2713–28

[70] Straub W O 2006 *Simple Derivation of the Weyl Conformal Tensor*

[71] Kozameh C, Newman E, gravitation K T-G relativity and and 1985 undefined 1985 Conformal Einstein spaces *Springer*

[72] Straumann N 2013 General Relativity (Graduate Texts in Physics) *Springer* (Springer)

[73] Penrose R 2005 *The Road to Reality: A Complete Guide to the Laws of the Universe*

[74] Lachì Eze-Rey M and Luminet J-P 2003 COSMIC TOPOLOGY *arXivgr-qc/9605010v2 9 Jan 2003*

[75] Ellis G F R and van Elst H 1998 Cosmological models (Carg\`{e}se lectures 1998)

[76] M. P. Hobson, Hobson/Efstathiou/Lasenby, G. P. Efstathiou A N L General Relativity - Google Books

[77] Ryden B 2006 *Introduction to Cosmology* (San Francisco, CA, USA: Addison Wesley, ISBN 0-8053-8912-1.)

[78] Chen G C F, Fassnacht C D, Suyu S H, Rusu C E, Chan J H H, Wong K C, Auger M W, Hilbert S, Bonvin V, Birrer S, Millon M, Koopmans L V E, Lagattuta D J, McKean J P, Vegetti S, Courbin F, Ding X, Halkola A, Jee I, Shajib A J, Sluse D, Sonnenfeld A and Treu T 2019 A SHARP view of H0LiCOW: H0 from three time-delay gravitational lens systems with adaptive optics imaging *Mon. Not. R. Astron. Soc.* **490** 1743–73

[79] Dainotti M G, De Simone B, Schiavone T, Montani G, Rinaldi E and Lambiase G 2021 On the Hubble Constant Tension in the SNe Ia Pantheon Sample *Astrophys. J.* **912** 150

[80] Copi C J, O'Dwyer M and Starkman G D 2016 The ISW effect and the lack of large-angle CMB temperature correlations *Mon. Not. R. Astron. Soc.* **463** 3305–10

[81] Aguado D S, Ahumada R, Almeida A, Anderson S F, Andrews B H, Anguiano B, Ortíz E A, Aragón-Salamanca A, Argudo-Fernández M, Aubert M, Avila-Reese V, Badenes C, Rembold S B, Barger K, Barrera-Ballesteros J, Bates D, Bautista J, Beaton R L, Beers T C, Belfiore F, Bernardi M, Bershady M, Beutler F, Bird J, Bizyaev D, Blanc G A, Blanton M R, Blomqvist M, Bolton A S, Boquien M, Borissova J, Bovy J, Brandt W N, Brinkmann J, Brownstein J R, Bundy K, Burgasser A, Byler N, Diaz M C, Cappellari M, Carrera R, Sodi B C, Chen Y, Cherinka B, Choi P D, Chung H, Coffey D, Comerford J M, Comparat J, Covey K, da Silva Ilha G, da Costa L, Dai Y S, Damke G, Darling J, Davies R, Dawson K, de Sainte Agathe V, Machado A D, Moro A Del, de Lee N, Diamond-Stanic A M, Sánchez H D, Donor J, Drory N, des Bourboux H du M, Duckworth C, Dwelly T, Ebelke G, Emsellem E, Escoffier S, Fernández-Trincado J G, Feuillet D, Fischer J L, Fleming S W, Fraser-McKelvie A, Freischlad G, Frinchaboy P M, Fu H, Galbany L, Garcia-Dias R, García-Hernández D A, Oehmichen L A G, Geimba Maia M A, Gil-Marín H, Grabowski K, Gu M, Guo H, Ha J, Harrington E, Hasselquist S, Hayes C R, Hearty F, Toledo H H, Hicks H, Hogg D W, Holley-Bockelmann K, Holtzman J A, et al 2018 The fifteenth data release of the sloan digital sky surveys: First release of manga derives quantities, data visualization tools and stellar library *arXiv* **55** 23

[82] Chiang Y-K, Makiya R, Ménard B and Komatsu E 2020 The Cosmic Thermal History Probed by Sunyaev-Zeldovich Effect Tomography *arXiv*

[83] Kashlinsky A, Atrio-Barandela F and Ebeling H 2011 Measuring the dark flow with public X-ray cluster data *Astrophys. J.*

732 1–7

[84] Hoffman Y, Pomarède D, Tully R B and Courtois H M 2017 The dipole repeller *Nat. Astron.* **1** 1–5

[85] Dupourqué S, Tibaldo L and Von Ballmoos P 2021 Constraints on the antistar fraction in the Solar System neighborhood from the 10-year Fermi Large Area Telescope gamma-ray source catalog *Phys. Rev. D* **103** 083016

[86] Khlopov M Y, Kirichenko A O and Mayorov A G 2020 Anihelium flux from antimatter globular cluster

[87] Poulin V, Salati P, Cholis I, Kamionkowski M and Silk J 2019 Where do AMS-02 anti-helium events come from? *Proceedings of Science* vol 364 (Sissa Medialab Srl) p 074

[88] Kassin S A, Weiner B J, Faber S M, Gardner J P, Willmer C N A, Coil A L, Cooper M C, Devriendt J, Dutton A A, Guhathakurta P, Koo D C, Metevier A J, Noeske K G and Primack J R 2012 THE EPOCH OF DISK SETTLING: z ~ 1 TO NOW *Astrophys. J.* **758** 106

[89] Kassin S A, Brooks A, Governato F, Weiner B J and Gardner J P 2014 *KINEMATIC EVOLUTION OF SIMULATED STAR-FORMING GALAXIES*

[90] Guo Q, Hu H, Zheng Z, Liao S, Du W, Mao S, Jiang L, Wang J, Peng Y, Gao L, Wang J and Wu H 2019 Further evidence for a population of dark-matter-deficient dwarf galaxies *Nat. Astron.* **4** 246–51

[91] van Dokkum P, Danieli S, Abraham R, Conroy C and Romanowsky A J 2019 A Second Galaxy Missing Dark Matter in the NGC 1052 Group *Astrophys. J.* **874** L5

[92] Danieli S, van Dokkum P, Conroy C, Abraham R and Romanowsky A J 2019 Still Missing Dark Matter: KCWI High-resolution Stellar Kinematics of NGC1052-DF2 *Astrophys. J.* **874** L12

[93] DES Collaboration, Abbott T M C, Aguena M, Alarcon A, Allam S, Alves O, Amon A, Andrade-Oliveira F, Annis J, Avila S, Bacon D, Baxter E, Bechtol K, Becker M R, Bernstein G M, Bhargava S, Birrer S, Blazek J, Brandao-Souza A, Bridle S L, Brooks D, Buckley-Geer E, Burke D L, Camacho H, Campos A, Rosell A C, Kind M C, Carretero J, Castander F J, Cawthon R, Chang C, Chen A, Chen R, Choi A, Conselice C, Cordero J, Costanzi M, Crocce M, da Costa L N, Pereira M E da S, Davis C, Davis T M, De Vicente J, DeRose J, Desai S, Di Valentino E, Diehl H T, Dietrich J P, Dodelson S, Doel P, Doux C, Drlica-Wagner A, Eckert K, Eifler T F, Elsner F, Elvin-Poole J, Everett S, Evrard A E, Fang X, Farahi A, Fernandez E, Ferrero I, Ferté A, Fosalba P, Friedrich O, Frieman J, García-Bellido J, Gatti M, Gaztanaga E, Gerdes D W, Giannantonio T, Giannini G, Gruen D, Gruendl R A, Gschwend J, Gutierrez G, Harrison I, Hartley W G, Herner K, Hinton S R, Hollowood D L, Honscheid K, Hoyle B, Huff E M, Huterer D, Jain B, James D J, Jarvis M, Jeffrey N, Jeltema T, Kovacs A, Krause E, Kron R, Kuehn K, Kuropatkin N, Lahav O, Leget P-F, Lemos P, et al 2021 Dark Energy Survey Year 3 Results: Cosmological Constraints from Galaxy Clustering and Weak Lensing **54** 30

[94] Burkert A, Schartmann M, Alig C, Gillessen S, Genzel R, Fritz T K and Eisenhauer F 2012 Physics of the galactic center cloud G2, on its way toward the supermassive black hole *Astrophys. J.* **750** 58

[95] Becerra-Vergara E A, Argüelles C R, Krut A, Rueda J A and Ruffini R 2021 Hinting a dark matter nature of Sgr A* via the S-stars *Mon. Not. R. Astron. Soc. Lett.* **505** L64–8

[96] Shen Y 2009 Supermassive black holes in the hierarchical universe: A general framework and observational tests *Astrophys. J.* **704** 89–108

[97] Wang Q D 2021 Chandra large-scale mapping of the Galactic Centre: probing high-energy structures around the central molecular zone *Mon. Not. R. Astron. Soc.* **504** 1609–18

[98] Heywood I, Camilo F, Cotton W D, Yusef-Zadeh F, Abbott D, Adam M, Aldera M A, Bauermeister F, Booth S, Botha A G, Botha D H, Brederode L S, Brits Z B, Buchner S J, Burger J P, Chalmers J M, de Villiers D, Dikgale-Mahlakoana M A, du toit L J, P esterhuyse S W, Fanaroff B L, Foley A, Fourie D J, Gamatham G, Goedhart S, Gounden S, Hlakola M J, Hoek C J, Hokwana A, Horn D M, G Horrell J M, Hugo B, Isaacson A, Jonas J L, B L Jordaan J D, Joubert A F, G Józsa G I, Julie P M, Kapp F B, Kenyon J S, A Kotzé P P, Kriel H, Kusel W, Liebenberg D, Loots A, Lunsky B M, Macfarlane P S, Magnus L G,

Magozore C M, Mahgoub O, L Main J P, Malan J A, Malgas D, Manley J, J Maree M D, Merry B, Mnyandu N, Moeng I P, Mphego M C, New W S, Ngcebetsha B, Oozeer N, Otto A J, Passmoor S S, Patel A A, Peens-Hough A, Perkins S J, ratcliffe S M, rust A, Salie S, Schwardt L C, Serylak M, Sirothia S K, Smirnov O M, Sofeya L, Swart P S, tasse C, taylor D, theron I P, thorat K, tiplady A J, tshongweni S, van Balla J, van der Byl A, van der Merwe C, van Dyk C L, rooyen V, Van tonder V, Wyk V, Wallace B H, Welz M G and Williams L P Inflation of 430-parsec bipolar radio bubbles in the Galactic Centre by an energetic event *Nature*

[99] Wittenburg N, Kroupa P and Famaey B 2020 The formation of exponential disk galaxies in MOND *Astrophys. J.* **890** 173

[100] Pavel Grinfeld 2013 *Introduction to Tensor Analysis and the Calculus of Moving Surfaces* (Springer)

[101] Krishnan V V, Bailes M, Van Straten W, Wex N, Freire P C C, Keane E F, Tauris T M, Rosado P A, Bhat N D R, Flynn C, Jameson A and Osłowski S 2020 *Lense-Thirring frame dragging induced by a fast-rotating white dwarf in a binary pulsar system*

[102] Wang P, Libeskind N I, Tempel E, Kang X and Guo Q 2021 Possible observational evidence that cosmic filaments spin *Nat. Astron.* 1–7

[103] Feng W-X, Yu H-B and Zhong Y-M 2021 Seeding Supermassive Black Holes with Self-interacting Dark Matter: A Unified Scenario with Baryons *Astrophys. J. Lett.* **914** L26

[104] Sam Reid et al 2013 Fluid Pressure and Flow, PhET Interactive Simulations.